Université du Québec
à Rimouski

ÉCOLOGIE ET PERFORMANCE PHOTOSYNTHÉTIQUE DU PHYTOPLANCTON PENDANT UN CYCLE DE MARÉE VIVE-EAU/MORTE-EAU, DANS LE FRONT DU SUD DU GOLFE SAN JORGE, PATAGONIE

Memoire présenté

dans le cadre du programme de maîtrise en océanographie

en vue de l'obtention du grade de maître ès sciences

par

Flores Melo Ximena Elizabeth ©

Janvier 2018

Composition du jury :

Daniel Bourgault, membre du jury interne, Université du Québec à Rimouski
Maurice Levasseur, membre du jury externe, Université Laval

Sous la direction de :

Gustavo A. Ferreyra, Université du Québec à Rimouski
Irene Schloss, Université du Québec à Rimouski/Instituto Antártico Argentino
Cédric Chavanne, Université du Québec à Rimouski
Gastón Almandoz, Consejo Nacional de Investigaciones Científicas y Técnicas

Dépôt initial le 14 août 2017 Dépôt final le 14 Janvier 2018

Dedicación

A mi mamá Jorgina Melo y mi papá Rafael Flores,
por darme alas, y a mi novio, Daniel Gasco,
por acompañarme en el vuelo

Dédicace

À ma maman, Jorgina Melo et mon papa Rafael Flores,
pour me donner des ailes, et à mon copin,
Daniel Gasco, pour voler avec moi.

Remerciements

Je remercie les institutions qui ont rendu ce project possible et qui m'ont soutenu financièrement: Bec.Ar, MinCyT, CONICET, Gobierno de la provincia de Chubut en Argentine, UQAR et ISMER au Canada, et aussi le Service aux étudiants de l'UQAR et QuébecOcéan. Merci aux membres de jury, Daniel Bourgault et Maurice Levasseur, pour leur engagement et leur temps. Merci à mes directeurs Gustavo Ferreyra, Irene Schloss, Cédric Chavanne et Gaston Almandoz pour m'avoir motivé et appuyé à tous moments et quelque soit la distance, pour m'avoir patiemment écouté et débattu chaque idée jusqu'à en rire. Je les remercie de m'avoir montré que la science n'est pas facile, qu'il faut faire beaucoup d'efforts, mais surtout qu'il faut garder du temps pour la vie en famille, avec les amis, et pour courir. Je remercie aux professeurs Dany Dumont et Luis-Phillipe Nadeau pour leurs précieux commentaires et apports. Merci à l'équipe technique de l'ISMER, Pascal Guillot, James Caveen, Mélanie Simard, Claude Belzile, Pascal Rioux, et Dominique Lavallée. Un grand merci à Martine Belzile, pour son aide et pour avoir su lire dans mes pensées quand mon français était déficient. Merci aux scientifiques, Valérie Massé-Beaulne, Américo Torres, Gabriela Williams, Noela Alvarez, Maité Latorre qui m'ont aidé pour l'analyse des échantillons et qui m'ont apporté des informations essentielles pour l'interprétation des résultats.

Merci à mes belles amies argentines qui ont partagé avec moi cette aventure de réaliser une maîtrise à Rimouski: Maité Latorre, Eloisa Gimenez, Julieta Kaminsky. À mes amis latino-americains: Maria (Yiya) et Santi (superhéroe), et au gang argentin à Rimouski: Claudia, Alejandro et Mati, Aru, Daniel Mareque et sa famille, Rosana Modino et sa famille, Jesi, Nacho et Licho. Merci aussi aux formidables amis de maîtrise, avec qui j'ai partagé à la fois les bons moments et aussi les moments de stress: Nais, Enzo, Maude, Valentin, Antoine, Grégoire, Phillu, Antony, Elsa, et les filles argentines Andy, Maga, Bel, Marian. Merci aussi à tous qui ont rendu possible la formation «des étrangers», et pour tous les moments privilégiés qu'on a vécu ensembles. Merci aux personnes qui m'ont accueilli: Juano, Leo B, David, et surtout ma belle famille adoptive: Maria et Jeff et leurs filles, Mélia

et Danaé. Merci à tous ceux qui étaient loin de Rimouski, mais qui étaient toujours présents: à mes directeurs/directrice et amis du Centro Regional Universitario de Bariloche, du Laboratorio de calidad de aguas, Mónica Diaz, Gustavo Baffico, Fernando Pedrozo, pour m'avoir formé avec beaucoup de patience.

Je veux surtout remercier ceux qui ont fait ce que je suis, à ma famille, ma maman Jorgina Melo et mon papa Rafael Flores, pour m'avoir motivé dès le début de mes études, pour leurs encouragements et leurs conseils. Mes frères et soeurs, particulièrement, Hugo, mon frère ainé, pour son appui et son attention. Merci aussi à mon grand père Rafael, mon oncle Luis et ma tante Susana, pour avoir été toujours présents et avoir pris soin de moi. Finalement à mon ami et compagnon de vie, Daniel Gasco, je dis simplement merci pour m'accompagner dans mes études; tu as été mon grand soutien émotionnel.

Table des matiéres

Liste des tableaux

Tableaux des figures

Liste des abréviations, des sigles et des acronymes

Chl-a	Chlorophyll *a*
CTD	Conductivity – Temperature - Depth
$\mathscr{N}^2$	Brunt – Väisälä frequency
PAR	Photosynthetic Available Radiation
POC	Particulate Organic Carbon
PON	Particulate Organic Nitrogen
POM	Particulate Organic Matter
ROTV	Remotely Operated Towed Vehicle
SJG	San Jorge Gulf
SST	Sea Surface Temperature
$\mathbf{Z_{eu}}$	Euphotic Depth

1. Résumé

Les fronts des marées sont des interfaces qui séparent des eaux stratifiées plus profondes des eaux mélangées moins profondes, où les courants de marée fournissent l'énergie turbulente pour mélanger la colonne d'eau pouvant pouvant éroder la pycnocline dans les zones moins profondes. En général, la zone stratifiée présente des concentrations en nutriments plus faibles dans la couche de surface que dans la zone mélangée. On s'attend donc à trouver différents assemblages de phytoplancton entre la zone mélangée et la zone stratifiée du front. Le front du sud du Golfe San Jorge, en Argentine, a été étudié pendant un cycle de marée de vive-eau/morte-eau, en considérant les gradients horizontaux de densité, les courants de marées et la bathymétrie. La position et la forme du front sont influencées par des instabilités baroclines, qui jouent probablement un rôle important dans le transport horizontal de nutriments à travers le front. Nous avons étudié le phytoplancton en utilisant un critère basé sur l'espectre de tailles : micro-phytoplancton, nano-phytoplancton, pico-phytoplancton et cyanobactéries. À son tour, les hétérotrophes ont été classifiés comme suit: dinoflagellés (hétérotrophes et mixotrophes), ciliés et bactéries. La plus forte concentration de biomasse phytoplanctonique a été trouvée du côté stratifié pendant la marée de morte-eau, où les groupes phytoplanctoniques les plus petits, composés de pico- et nano-phytoplancton et cyanobactéries, apportent la plus grande contribution de carbone à la biomasse totale. La biomasse hétérotrophique la plus importante est apportée par les bactéries. Pendant la marée de vive-eau, dans la zone stratifiée, la plus grande contribution de carbone est apportée par les cellules micro-phytoplanctoniques : constitué principalement par dinoflagellés et diatomées. Le carbone des hétérotrophes est principalement apporté par les grands cellules comme les ciliés et les dinoflagellés. La zone mélangée montre des résultats remarquables par rapport à l'état physiologique des cellules, qui présentent une photo-acclimatation de leur système photosyntétique aux conditions optimales de lumière présents à des profondeurs moyennes de la colonne d'eau. Ce résultat suggère que les cellules photo-inhibées en surface sont advectées par les mouvements turbulents verticaux à des profondeurs où les conditions de lumière sont optimales et de manière similaire, les cellules sous la zone euphotique sont transportées aux profondeurs lumineuses. Ces résultats nécessiterait des observations à plus long term sur un grand nombre de cycles de marée vive-eau / morte-eau, car il n'est pas possible d'armer que les observations analyses dans ce memoire soient représentatives d'un cycle typique de marée vive-eau / morte-eau.

Mots-clés : front de marées, marée vive-eau, marée morte eau, densité, zone mélangée, zone stratifiée, transport des nutriments, phytoplancton, biomasse, état physiologique.

2. Abstract

Tidal fronts are interfaces separating stratified deepest waters from the mixed shallowest waters, where tidal currents provide enough turbulent energy to mix the entire water column and to overcome stratification in shallow zones. The stratified side is characterized by lower inorganic nutrients concentrations in the surface layer than the mixed side. Therefore, phytoplankton assemblages are expected to be quantitatively or qualitatively different from one side to the other of the front. The front in the South of San Jorge Gulf (SJG), Argentina, was characterized during a spring-neap tidal cycle considering horizontal gradients of density, tidal currents and bathymetry. It was found that baroclinic instabilities influence the shape and position of the front and presumable play an important role in the horizontal nutrient transport across the front. The phytoplankton was categorized according with sizes spectre: microphytoplankton, nanophytoplankton, picophytoplankton and cyanobacteria. In turn, the heterotrophs were categorized as: dinoflagellates (heterotrophs and mixotrophs), ciliates and bacteria. The highest phytoplankton biomass concentrations were found in the stratified side of the front during neap tide. Under such conditions, the main contributors to the total autotrophic biomass were the smallest size groups as pico-phytoplankton and cyanobacteria and nanophytoplankton. The main contribution to heterotrophic biomass was mainly bacteria. On the other hand, the stratified side during spring tide showed a higher contribution of carbon from bigger microphytolankton cells than during neap tide, corresponding to dinoflagellates and diatoms. This side of the front presented the largest heterotrophic cells, such as ciliates and heterotrophic dinoflagellates. The mixed side is not less important, as shown by the physiological state of autotrophs. Indeed, cells present in well-mixed waters photo-acclimate their photosynthetic system to an optimum of light conditions, suggesting that cells near the surface, which are probably photo-inhibited, and cells below the euphotic zone, which are light-deprived, are quickly advected by turbulent vertical motions to the depth range with optimal irradiance conditions. This results need observations over many spring-neap tidal cycles, because the observations in this study could not be representative of the typical spring-neap tidal cycle.

Keywords : tidal front, spring tide, neap tide, density, mixed side, stratified side, nutrients transport, phytoplankton, biomass, physiological state.

ÉCOLOGIE ET PERFORMANCE PHOTOSYNTHÉTIQUE DU PHYTOPLANCTON PENDANT UN CYCLE DE MARÉE VIVE-EAU/MORTE-EAU, DANS LE FRONT DU SUD DU GOLFE SAN JORGE, PATAGONIE

3. Introduction

3.1 Les fronts océaniques

Dans la plupart des océans, des variables telles que la température et la salinité changent d'une manière relativement marqués dans l'échelle horizontale. Ces zones définent des fronts. Les front sont des zones avec des gradients horizontaux évident, qui agissent comme des interfaces entre différentes masses d'eau (Acha et al, 2015).

Les fronts présentent des phénomènes dynamiques à différentes échelles temporelles et spatiales qui abritent des processus biologiques et écologiques particuliers (Owen, 1981; Mann et Lazier, 1996). Il est parfois possible d'observer les fronts à la surface sans même effectuer des mesures, grâce à l'accumulation de matériel flottant lié au gradient maximal de densité, ou grâce au changement de la couleur de l'eau dû aux différentes concentrations de chlorophylle *a* (Chl-*a*) dans les eaux des deux côtés du front, résultat de différences dans l'activité biologique (Simpson et Hunter, 1974).

Les fronts ont été observés et décris depuis le 19e siècle par différents scientifiques et voyageurs, comme par exemple Charles Darwin en 1845, et des pêcheurs qui avaient observé une haute activité biologique autour des fronts (Acha et al., 2015). Ils existent différents types de fronts, comme les fronts de marées, les fronts thermo-halins, les fronts produits par remontées d'eau (*upwellings*), les fronts estuariens, les fronts de panaches, les

fronts associés aux convergences ou divergences de masses d'eaux dans l'océan, les fronts associés aux tourbillons et les fronts associés aux caractéristiques topographiques comme les caps, les îles ou les canyons (Mann et Lazier, 1996).

3.2 Les fronts de marées

Les fronts de marées se trouvent parmi les plus étudiés, ils sont saisonniers et s'établissent chaque année, à peu près au même moment et à la même place (Acha et al., 2015). Dans les régions tempérées côtières, où la colonne d'eau devient stratifiée en été, les courants de marées fournissent l'énergie nécessaire pour éroder la pycnocline, en diminuant la stabilité de la colonne d'eau (Landeira et al., 2014; Acha et al. 2015). Les masses d'eau dans la région stratifiée des fronts ont généralement deux régimes différents de mélange qui leurs sont associés et qui résultent en une couche supérieure mélangée, une couche mélangée de fond et, entre elles, un gradient plus ou moins fort de densité, la pycnocline. La turbulence dans la première couche est influencée par le vent, tandis que dans la couche de fond elle est influencée par les courants de marée. La pycnocline se maintient quand ni le vent, par dessus, ni les courants par dessous, sont suffisants pour mélanger la couche de surface avec les eaux profondes et, par conséquent, la colonne d'eau reste stratifiée (Pingree et al., 1978).

La turbulence générée par les courants de marées, étant due à la friction sur le fond, diminue vers la surface et ne peut ainsi éroder la pycnocline lorsque la colonne d'eau est trop profonde. Par contre, dans les eaux moins profondes, la colonne d'eau demeure mélangée pendant tout le cycle de marée, même quand l'énergie turbulente est minimale (Loder et Platt, 1985). En conséquence, un front de marées est une zone de séparation entre des eaux stratifiées plus profondes et des eaux mélangées moins profondes (Figure 1). La position de cette séparation, c'est-à-dire, la position frontale dépend, entre autres variables,

de l'énergie des marées et de la bathymétrie (Simpson et Hunter 1974; Owen, 1981; Franks, 1992).

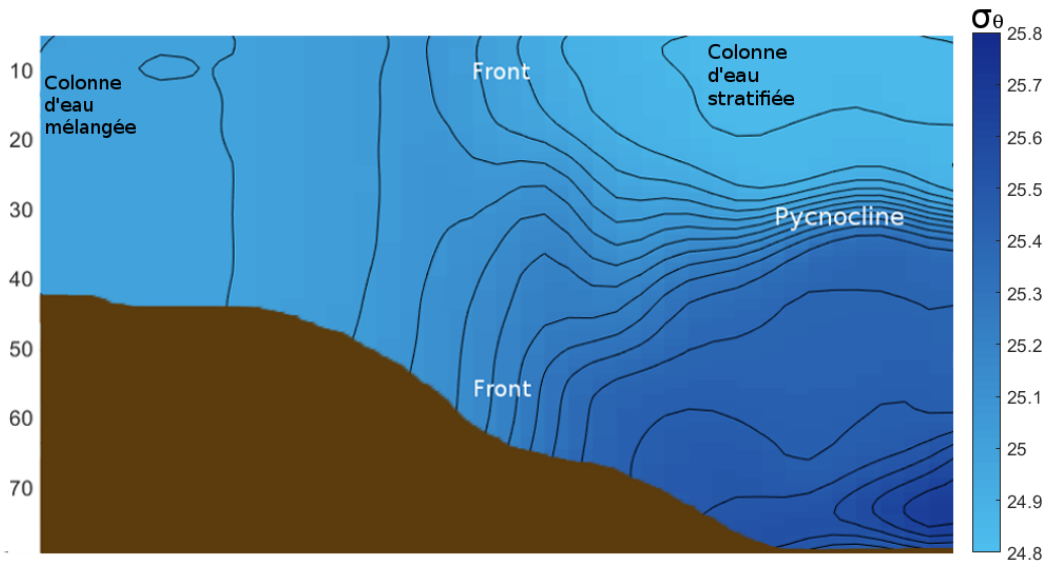

Figure 1: Structure d'un front de marée

3.3 Le cycle de marée vive-eau /morte-eau

Les marées sont génerées par les forces gravitationnelles gérées par la lune et le soleil sur les océans. Ses effects sont plus évidents dans les zones cotières et ont été étudiés pour les marins et par plusieurs scientifiques tel que Galileo, Descartes, Kepler, Newton, Euler, Bernoulli, Kant, Laplace, Airy, Lord Kelvin, Jeffreys, Munk (Stewart 2008). Les marées ont été caracterisées par leurs périodes qui se divisent en trois catégories : i) la période de 12.42 heures ou semi-journalière, ii) la période de 24 heures ou journal et iii) la période de plus de 24 heures ou long périodes (Mann et Lazier, 1996).

Quand le soleil et la lune sont alignées avec la Terre généront la plus haute élévation du niveau de la mer, appelée marée de vive-eau, qui se produit deux fois par mois. Mais

quand la lune est perpendiculaire à l'axe Terre-Soleil, les forces d'attraction de la lune et du soleil s'annulent partiellemente, et en conséquence produiront les niveaux de la mer les plus bas ou marée de morte-eau, aussi deux fois par mois (Talley, L. D. 2011).

3.4 Instabilités baroclines

Comme c'est le cas dans tous les fronts de densité, des instabilités baroclines peuvent se développer et engendrer des tourbillons (Loder et Platt, 1985; Mann et Lazier, 1996). Les tourbillons peuvent persister pendant quelques jours et jouer un rôle important dans les échanges des propriétés chimiques et biologiques au travers du front (Pingree, 1979). De plus, ces structures de méso-échelle sont importantes parce qu'ils peuvent contrôler la taille des cellules phytoplanktoniques (Rodriguez et al., 2001).

3.5 Nutriments

Les travaux de Simpson et Hunter (1974) montrent que l'eau de surface du côté mélangé des fronts sont plus riches en nutriments inorganiques (nitrates, phosphates, silicates, ammonium) que celle du côté stratifié, à cause du réapprovisionnement en nutriments provenant des eaux profondes lequel est limité du côté stratifié. En revanche, la zone mélangée du front apporte des nutriments de fond vers la surface mais, inversement, transporte les organismes autotrophes vers les eaux limitées en lumière (Pingree et al., 1978).

Cependant, l'approvisionnement de nutriments n'est pas seulement vertical dans les fronts de marées. Les mécanismes d'échange horizontaux peuvent devenir importants. Le modèle proposé par Loder et Platt (1985) permet d'estimer l'approvisionnement de nutriments de la surface de la zone mélangée, pendant les marées de vive-eau, vers la couche de surface de la zone stratifiée pendant la marée morte-eau à cause du déplacement

du front vers les eaux moin profondes, en considérant que les nutriments de la zone mélangée resteront confinés dans la couche supérieure de mélange quand la stratification avance due à la marée de morte-eau.

Cependant, ce modèle ne considère pas les échanges horizontaux associés aux tourbillons. En alternative à Loder & Platt (1985), Pingree (1979) propose un autre modèle qui permet d'estimer le flux de nutriments au travers du front associé aux tourbillons.

3.6 Le phytoplancton dans un front de marées

Pour comprendre la relation entre les fronts et l'accumulation du phytoplancton, il faut comparer les échelles temporelles associées aux processus physiques par rapport à celles associées à la croissance du phytoplancton sous les conditions d'un front, c'est-à-dire la disponibilité des nutriments et de lumière dans la colonne d'eau (Mann et Lazier, 1996).

Les concentrations maximales de Chl-*a* (considérée comme un proxy de la biomasse du phytoplancton) sont, généralement, trouvées dans la couche de surface du côté stratifié des fronts de marée (Pingree et al., 1978; Landeira et al., 2014), et décroissent en s'éloignant de l'interface frontale (Franks, 1992). Les échelles temporelles associées aux cycles des marées semi mensuells influencent la distribution de la Chl-*a* dans et autour des fronts (Owen, 1981). Ceci est lié aux effets des marées sur les variations dans la disponibilité des nutriments à travers le front ainsi qu'à la profondeur de la couche euphotique, définie comme la profondeur moyenne à laquelle l'irradiance atteint 1% de l'irradiance incidente dans la surface (Reynolds 2006). Ce mécanisme favorise le développement des zones de haute productivité primaire et la identification des différentes assemblages du phytoplancton (Margalef, 1978).

La structure de la communauté phytoplanctonique dans un front de marées est prédictible et la présence des principaux groupes dépend de l'accessibilité aux eaux riches

en nutriments inorganiques nouveaux (nitrates), ou régénérés (ammonium) à partir de la matière organique décomposée par les bactéries (Pingree et al., 1978; Frank 1992).

Selon Glibert (2016), dans la zone où l'énergie turbulente est grande, les nutriments inorganiques dissous sont disponibles et le rapport N:P est grand, en considérant que ce ratio balancé est égal à 16 (Redfield, 1934), ce qui favorise le développement de certains groupes, principalement les diatomées. En revanche, en zone stratifiée, où l'énergie turbulente est moins forte, est caractérisée par la présence de groupes comme les dinoflagellés et les flagellés plus grands que 20µm (micro – dinoflagellés et micro flagellés). Cependant, les cellules plus petites que 20µm seront plus importantes que les micro-dinoflagellés et micro-flagellés si la zone stratifiée présente un faible rapport de N:P (Glibert, 2016).

La matière organique dérivée du phytoplancton, à la base du réseau trophique marin, est riche en protéines, en hydrates de carbone, et en lipides (Copin-Montegut et Copin-Montegut, 1983). Sa valeur nutritionnelle, en conséquence, est importante pour les niveaux supérieurs. Le rapport entre le carbone organique particulaire (COP) et l'azote organique particulaire (AOP), ou rapport C:N, peut être utilisé comme une approximation de la qualité en termes alimentaires de la matière organique disponible pour les niveaux trophiques supérieurs. Dans le cas de la matière organique dérivée de la productivité primaire, le rapport C:N présente les plus basses valeurs, autour de 4, en signalant un enrichissement en azote, et en conséquence, une matière organique avec une valeur nutritionnelle relativement plus haute (Geider et La Roche, 2002; Townsend et Thomas, 2002). Connaître la composition de la communauté phytoplanctonique est également essentiel car la quantité et la qualité de la production de matière organique par le processus de photosynthèse dépend de l'abondance relative des différentes espèces (Falkowski, 1980).

3.7 Le cas du sud du Golfe San Jorge

Le Golfe San Jorge (GSJ) (Figure 2) est délimité par le Cap Dos Bahías (44º55´S, 65º32´W) au nord et par le Cap Tres Puntas (47º06´S, 65º52´W) au sud, en couvrant une aire de 32.000 km^2. Le GSJ représente une importante zone de reproduction des oiseaux de mer (Yorio et al., 2010). Les principales activités autour du GSJ sont la pêche de la crevette *Pleoticus muelleri* et du merlu *Merluccius hubbsi* (Aubone et al., 2000; Glembocki et al., 2015). Malgré la création du Parc Marin inter-juridictionnel au nord du golfe, la pêcherie artisanale et les activités pétrolières offshores ainsi que l'écotourisme ont augmenté (Yorio, 2009). Pour cette raison le GSJ a été identifié comme une des aire stratégiques prioritaires de la recherche océanographique par le Ministère de la science et la technologie de l'Argentine (Programme Pampa Azul) pour la conservation des espèces marines et l'exploitation soutenable de la pêche (Paparazzo et al., 2017).

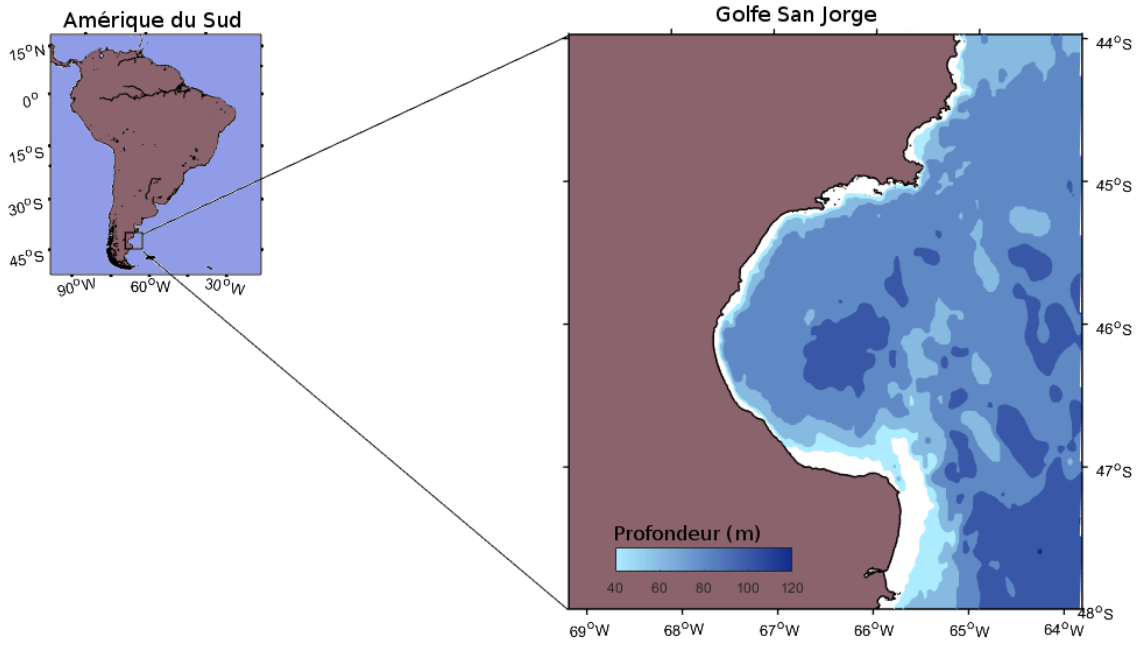

Figure 2: Le golfe San Jorge (Patagonie, Argentine)

Le GSJ est un bassin semi fermé où la circulation des courants est dominée par la marée et les forts vents du sud – ouest (Palma et al, 2004; Tonini et al., 2006). Le centre du golfe est la zone la plus profonde, atteignant jusqu'à 100 m (Fernández et al., 2008), alors que la zone du sud-est présente une élévation connue par les pecheurs comme "Le Mur", avec 60m de profondeur (Glemboki et al., 2015). Cette zone en particulier est caractérisée par une aire de haute dissipation d'énergie par les marées (Rivas et Pisoni, 2010).

3.8 Le front de marée du sud du Golfe San Jorge

Cette aire côtière de la Patagonie Argentine présente un front de marée typique des eaux tempérées (Fernández et al., 2005) qui a été caractérisé par différents auteurs en utilisant des méthodologies diverses, comme Glorioso et Flather (1995) avec le paramètre de Simpson and Hunter (1974), et par le gradient maximal de température de surface à partir d'images satellitaires (Bogazzi et al., 2005; Glembocki et al., 2015).

Le front du sud du GSJ sépare deux secteurs : premier, avec une faible profondeur et une haute activité de mélange par les marées, ne permettant pas le développement d'une stratification saisonnière dans la colonne d'eau. Ce secteur moins profond est associé à la zone côtière sud. Le deuxième secteur est plus profond, situé en direction à la zone centrale du golfe, et présente une faible influence de l'activité de la marée. Ce système d'eaux voisines, mélangées et stratifiées, permet la formation d'un front de marée avec des variations saisonnières très marquées (Cucchi-Colleoni et Carreto, 2001; Louge et al., 2004; Fernández et al., 2005; Tonini et al., 2006).

Pendant l'été, le front du sud du GSJ présente de grandes concentrations en Chl-*a*. Sa présence permet le développement d'une communauté benthique diversifiée (Fernández et al., 2005), et il est aussi une aire très importante de rétention de larves de la crevette rouge argentine (Glembocki et al., 2015). Malgré l'importance de la variabilité spatiale et temporelle pendant un cycle de marée vive-eau / morte-eau, et ses conséquences sur la

disponibilité des nutriments et sur les paramètres clés du phytoplancton, comme la composition de la communauté, l'accumulation du carbone et les réponses physiologiques, les études sur ces processus dans le sud du GSJ n'existent pas.

3.9 Objectifs

Dans le contexte précédent, les trois objectifs de ce projet sont d'abord de caractériser la variabilité temporelle des positions du front pendant un cycle de marée morte-eau/ vive-eau, et sa variabilité spatiale en relation avec la bathymétrie. Ensuite, nous chercherons à comprendre comment les changements physiques impactent la disponibilité des nutriments dans la couche de surface de la colonne d'eau. Finalement, nous étudierons comment la communauté du phytoplancton répond à ces variables physiques et chimiques dans la zone frontale, en considérant l'accumulation de carbone, la distribution des principaux groupes de phytoplancton, leur état physiologique et leurs relations avec la communauté micro-, nano-, et pico-hétérotrophique.

3.10 Cadre du projet

Cette étude a été menée dans le cadre du projet PROMESSE (Programme multidisciplinaire de recherche en océanographie pour l'étude de l'écosystème, de la géologie Marine du Golfe San Jorge et de la côte de la province de Chubut; Patagonie argentine), un accord bilatéral entre l'Argentine et le Canada, avec la participation du Ministerio de Ciencia, Teconología e Innovación Productiva de la República Argentina (MINCyT- En français : Ministère de Science, Téchnologie et Innovation Productif), la province du Chubut, le Consejo Nacional de Investigaciones Científicas y Técnicas (CONICET) et l'Université du Québec à Rimouski/Institut des sciences de la mer de Rimouski (UQAR/ISMER). Cette recherche a été effectuée abord du navire *R/V Coriolis II*

durant l’été austral 2014. L’objectif central de ce projet de Maîtrise a été spécifiquement d’étudier le front de marée du sud du GSJ pendant un cycle de marée semi-mensuel, en quantifiant des variables physiques (lumière, densité, stabilité de la colonne d'eau, courants de marées) et chimiques (nitrates, phosphates, silicates) du milieu, afin d’étudier ses effets sur la communauté phytoplanctonique, en considérant son abondance et biomasse, sa composition, sa distribution et des paramètres photosynthétiques clés des cellules.

Les résultats de cette étude ont été présenté dans divers réunions scientifiques. Une première présentation a été réalisée en 2015 à l'Assemblée Générale Annuelle (AGA) de Québec-Océan (Q-O). À cette occasion, une mention du jury a été obtenue à la meilleure présentation pour un poster de maîtrise. En plus, une présentation orale en 2016 a eu lieu aussi à l’AGA de Q-O. Finalement, une présentation orale a été effectuée dans un atelier de travail du projet PROMESSE dans la ville de Rimouski, en 2017.

Une présentation de groupe PROMESSE a été réalissée, sous le titre « *Navigons dans le Golfe San Jorge* » 13ème colloque de vulgarisation scientifique : La nature dans tous ses états, à Québec, Canada, en 2016.

PHYTOPLANKTON ECOLOGY AND PHOTOSYNTHETIC PERFORMANCE DURING A SPRING-NEAP TIDAL CYCLE IN THE SOUTHERN TIDAL FRONT OF THE SAN JORGE GULF, PATAGONIA.

4. Introduction

Marine fronts are transitional areas between two water masses with different properties (Simpson and Hunter, 1974; Acha et al., 2015). Fronts are thus regions of strong horizontal density gradients that originate when the pycnocline moves upward or downward (Simpson and Hunter, 1974; Franks, 1992; Bakun, 2006).

In temperate coastal regions, where the water column becomes stratified in summer, tidal currents provide turbulent energy which overcomes stratification (Landeira et al., 2014; Acha et al. 2015). Given that the strength of tidaly-induced mixing decreases from the bottom to the surface, the tidal energy has to be stronger to erode the pycnocline in deeper waters, while the shallowest coastal waters can remain mixed throughout the entire tidal cycle even during minimal turbulent energy periods (Loder and Platt, 1985). Consequently, a tidal front is a zone separating stratified deepest waters from the mixed shallowest waters, and the position of this zone depends on the tidal energy and the bottom depth (Simpson and Hunter 1974; Franks, 1992).

The pycnocline limits the upper layer at the stratified side of the front. When this horizontal boundary is shallower than the euphotic depth, the stratified side provides optimal irradiance conditions for photosynthetic organisms. However, the same boundary restricts the availability of inorganic nutrients in the upper layer, which are usually in higher concentrations in deeper waters. On the other hand, at the well-mixed side of the tidal front, mixing brings up inorganic nutrients from deeper waters to the euphotic layer but also transports phytoplankton cells to shaded depths (Pingree et al., 1978).

Nevertheless, horizontal displacements of these fronts can play an important role on nutrients distribution. Then, the horizontal advection of water and front displacements favor the input of nutrients in the surface layers (Landeira et al., 2014). Models have been developed to estimate the average rate of horizontal nutrient supply from the mixed zone during spring tide towards the upper mixed layer during neap tide (i.e. Loder and Platt, 1985).

Maximum chlorophyll-*a* (Chl-*a*) concentrations (a proxy for phytoplankton biomass) are usually found in the upper mixed layer at the stratified side of tidal fronts (Pingree et al., 1978; Landeira et al., 2014), decreasing away from the frontal interface towards offshore waters (Franks, 1992). The environmental variations in the frontal area, related to the upper mixed layer depth, the euphotic depth and the supply of nutrients, enhance primary production and allow the development of different phytoplankton assemblages (Margalef, 1978). For example, diatoms prefer inorganic nutrients, while dinoflagellates dominate in waters with available recycled inorganic compounds, resulting from bacterial remineralization or zooplankton excretion (Pingree et al., 1978; Gilbert, 2016, Reynolds 2006).

Glibert (2016), revisiting Margalef's mandala on interactions among dissolved inorganic nutrients, turbulence and light levels, suggested that it would be possible to predict which functional group of phytoplankton will be present along the environmental gradient across a frontal area: the well mixed side, the frontal boundary and the stratified side. Diatoms will be dominant when turbulent energy renders dissolved inorganic nutrients available in the euphotic layer so that the ratio N:P becomes largest (Glibert, 2016). Additionally, the stratified side of the front will be dominated by other microphytoplankton groups (>20µm) such as dinoflagellates and flagellates. However the smallest groups, such as pico-nanoeukariots and cyanobacteria (<20µm) will be more important than microphytoplankton if the stratified side has a lower N:P ratio.

Phytoplankton is essential for supporting marine trophic food webs, since they are located at the lowest level, producing new organic matter by photosynthesis (Falkowski, 1980). Particulate organic matter derived from phytoplankton has a high proteins, carbohydrates and lipids content (Copin-Montegut and Copin-Montegut, 1983), generally being of high nutritional value for higher trophic levels. A proxy of the nutritional quality of organic matter is the particulate carbon to nitrogen ratio (C:N) (Townsend and Thomas, 2002), which is low (i.e., high protein content) in prokaryotes assemblages (Caron et al., 1995).

4.1 The Southern tidal front of the San Jorge Gulf (SJG)

The SJG is a semi-closed basin where the center of the SJG is the deepest zone, reaching 100m. At south - east the gulf presents a bathymetry elevation called by the fishermen “The Wall”, where depth reaches 60m (Fernández et al., 2008; Glembocki, et al., 2015). The area is characterized by strong South-Western winds, recording mean wind speeds about 4.9 m/s at the meteorological station of the Comodoro Rivadavia (Coronato, 1997).

The SJG is characterizad by strong tides: its tidal energy is one of the highest in the world (Tonini et al., 2006). In particular, the south of the SJG exhibits the biggest tidal energy dissipation by bottom friction of Patagonia Argentina, the most intensive tidal currents with values ~3,5m/s with a-clockwise rotation (Tonini et al., 2006; Moreira et al., 2011). The M2 tidal constituent, which has a period of 12.42 hours, corresponding to a semi-diurnal cycle, can explain more than 80% of the tidal kinetic energy variance in the SJG (Rivas 1997; Mann et Lazier, 1996; Tonini et al., 2006; Palma et al., 2008).

A marked spatial temperature gradient is present in surface waters during the spring and summer seasons, revealing the presence of a tidal front (Louge et al., 2004). The formation of the thermocline occurs in spring, which it starts to decrease in late autumn

(Fernández et al., 2008). During summer time, the thermocline (which is the main factor contributing to vertical stratification in this area) reaches 30 to 50 m depth (Cucchi-Colleoni and D. Carreto, 2001).

The presence of this seasonal tidal front has been identified by satellite images (Fernández et al., 2005; Glembocki et al., 2015), as well as through the estimation of the Simpson-Hunter parameter (Glorioso and Flather, 1995) and modeling of tidal circulation and winds (Palma et al., 2004).

During the austral summer, the southern tidal front area exhibits high Chl-*a* concentrations (Rivas et al., 2006) and a diverse and abundant benthic community (Fernández et al., 2005). It is also considered as a significant area of larval retention of the Argentinean red shrimp (Glembocki, et al., 2015).

Despite the importance of front's spatial and temporal variability during spring and neap tidal cycles in other areas, which modulates nutrients dynamics and key phytoplankton parameters such as assemblages composition, carbon accumulation and photosynthetic responses, the understanding of these processes in the southern area of the SJG is still very limited. Furthermore, most investigations about tidal fronts are usually focused on the vertical nutrients fluxes (e.g., Li et al., 2012; Landeira et al., 2014), without considering the role of the horizontal fluxes in nutrient distribution.

In this context, the main goals of this work were i) to characterize the temporal variability of the front position during a spring-neap tidal cycle, and its spatial variability in relation to bathymetry; ii) to understand how this physical variability affects nutrients' availability in the upper layer of the water column, and iii) to investigate how the phytoplankton community responds to physical and chemical variations in the frontal zone, considering the distribution of the main phytoplankton groups, their carbon accumulation, photosynthetic state, and their relationship with micro-heterotrophs.

5. Material and Methods

5.1 Study area and sampling procedures

The frontal area located in the south-eastern of the San Jorge Gulf (SJG), Argentina, was studied during the *R/V Coriolis II* cruise in austral summer 2014, from February 5th to February 9th. Before the begining of sampling, the approximate location of the front was identified by the analysis of Sea Surface Temperature (SST) satellite images (see below. Figure 9). Eighteen cross-frontal transects and ten discrete rosette stations were performed to characterize the front and for discrete sampling of biological, physical and chemical variables, respectively (Figure 3). The first six transects and stations 1-5 were sampled on February 5, under spring tide conditions. The other twelve transects and stations 6-10, were sampled from February 8 to 9, during neap tide conditions.

5.2 Continuous data acquisition

Continuous water column sampling was performed with an undulating Remotely Operated Towed Vehicle (ROTV; ScanFish II), equipped with temperature and salinity (CTD, SBE-49) and fluorescence (WetLabs ECO FLNTU) sensors. Six 30-km long transects across the front were tracked respectively during the spring and neap tides periods, spaced 3 km from each other, approximately covering a total frontal region of 450 km^2 (Figure 3b, c). Previous to the six transects during neap tide, six overlapping transects were performed during twelve hours (Figure 3c), in order to characterize the frontal excursion caused by the semi diurnal tidal (M2 constituent) displacement. Horizontal current speed and direction were measured with a hull-mounted 150 kHz ADCP, and bottom topography was scanned with a hull-mounted Simrad EK-60 echosounder. Unfortunately, the ADCP was initially connected with a GPS that did not measure heading,

so currents could not be referenced to Earth coordinates. A GPS with coordinates data was connected to the ADCP on February 6 at 00:00 UTC during CTD station F3.

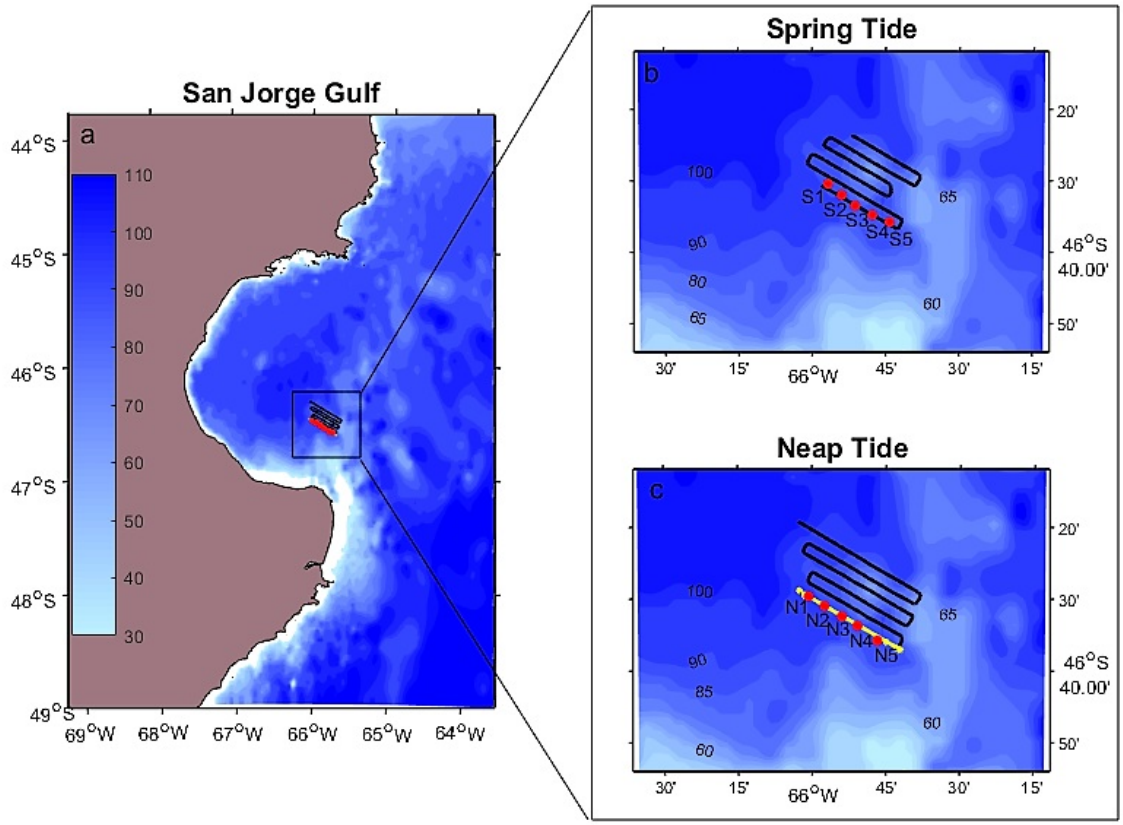

Figure 3: Map of the study area showing the location of SJG and sampling site in the frontal zone (a). (b and c) black lines are spaced transects and yellow line are superposed transects. Blue color gradient is bathymetry and red points are the stations during the spring (S1, S2, S3, S4, S5) and neap tide (N1, N2, N3, N4, N5).

5.3 Sea Surface Temperature (SST) satellite images

MODIS-Aqua Level-2 files were acquired from NASA ocean color web page (http://oceancolor.gsfc.nasa.gov) to evaluate the surface front positions in the water surface from February 4 to 10, with SST. This SST product uses the standard MODIS 11 µm non-linear sea surface temperature (NLSST) algorithm with coefficients derived by the Rosenstiel School of Marine and Atmospheric Science (RSMAS) and input SST guess from Reynolds OISST product (http://www.cdc.noa.gov/cdc/data.reynolds_sst.html).

5.4 Physical computations

Stratification strength was calculated using the Brunt–Väisäla frequency ($\mathcal{N}^2$) as (Equation 1):

$$N^2 = \frac{g}{\rho_0} \cdot \left(\frac{d\rho}{dz} \right) \quad \text{(Eq. 1)}$$

where g is the acceleration of gravity (9.8 m s $^{-2}$), ρ_0 is the standard density value of sea water (1025 kg m^{-3}), ρ is the potential density of sea water (kg m^{-3}) and z is the depth (m).

To create the figures of density and chlorophyll along a transect, the ROTV data was optimally interpolated to a regular grid of 50 x 80.

The surface front positions were identified as the latitude of the maximum horizontal density gradient.. This position was coincident with the 24.9 (kg m $^{-3}$) isopycnal at the 5 m depth, as shown in Figure 4. During neap tide, front positions were re-placed for tidal advection using currents measured by the shipborne ADCP. Currents were depth-averaged and projected on the transects direction. A sine curve at M2 frequency was least-square

fitted to each 12-hour survey to obtain semi-diurnal amplitudes and phases, which were used to compute tidal advection of front positions from a reference point along the transect corresponding to the passage of the MODIS satellite sensor.

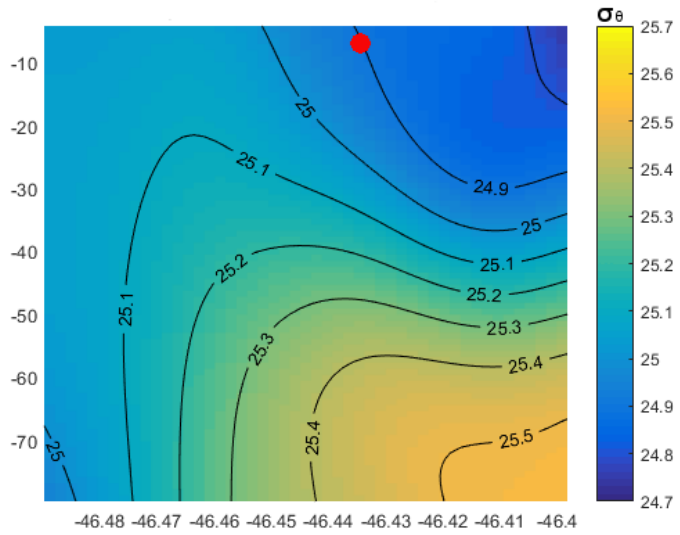

Figure 4: determination of the front position (red point) in the ROTV 6 th transect during spring tide. Axis *y* is depth (m), *x* is latitude and the color gradient is density.

Since the shipborne ADCP could not be geographically referenced during the spring tide survey, the following procedure was adopted. A sine curve at M2 frequency was least-square fitted to sea level observed at Comodoro Rivadavia station (Lat.: 45° 52' S, Long.: 67° 28' W, at ~70 km from the frontal zone) for each 12-hour survey during neap tide. The ratio of depth-average tidal current amplitude to sea level amplitude, and phase differences between currents and sea level, were similar for both surveys. It was therefore assumed that the amplitude ratio and phase difference between currents and sea level remain the same during a spring-neap cycle, allowing to infer tidal current amplitude and phase from sea

level amplitude and phase during spring tide. Front positions were then re-placed for tidal advection in the same way as during neap tide.

5.5 Profiling and discrete water column sampling

Vertical profiles of temperature (°C), conductivity (S m^{-1}) and depth (m) (CTD Sea-Bird SBE 911plus), fluorescence (WetLabs ECO FL; mg m^{-3}) and photosynthetic available radiation (LI-COR Biospherial PAR; µmol photon m^{-2} s^{-1}) were obtained from sensors attached to the rosette (Seabird Caroussel SBE-32 with 12x12L-bottles), which was lowered at 0.5 m s^{-1} vertical speed. The water column sampling on discrete stations was performed with 12 Niskin bottles of 12 L each installed on the rosette. Stations within each tidal period were located ~5 km from each other across the frontal zone, ensuring that both sides of the front would be sampled (Figure 3b and c). The downcast CTD profiles were used to define the Niskin bottles sampling depths during up-cast. Three out of the five stations performed during each tidal period (S3, S5, S1 for spring tide and N1, N3, N5 for neap tide) were sampled at Chl-*a* maximum depth to collect seawater. 100 ml samples were fixed with acidic Lugol and stored at 4°C in the dark until analyses of phytoplankton abundance, biomass and composition. Replicate 5 ml samples were in turn taken for phytoplankton and bacterioplankton flow cytometry studies. Samples were fixed with 20 µl of 25% Glutaraldehyde and stored at -80°C after 15 min of exposure to room temperature in the dark for further analyses. Incident irradiance (PAR) measurements were used to calculate the depth at which the 1% of the surface irradiance penetrates or Euphotic depth (Z_{eu}). With that purpose, the vertical attenuation coefficient (K_d) was calculated from the slope of the linear regression of the natural logarithm of PAR versus depth and then $Z_{eu} = 4.60514/K_d$ (Kirk 1983).

5.6 Nutrients

Water samples for nitrates, nitrites, phosphates and silicates determinations were collected at the same six stations than phytoplankton (i.e., S3, S5, S1, N1, N3, N5) at four different depths, two above (subsurface and Chl-*a* maximum) and two below the pycnocline (40-50 m and 70-80 m). Nutrients concentrations were determined using an Autoanalyzer following the Skalar protocols(Skalar Analytical, 2005) at the Centro Nacional Patagónico (CENPAT, Argentina, Strickland and Parson 1972).

The model of Loder & Platt (1985) (Equation 2) was used to estimate the nutrient's flux (Q_m: mmol m^{-1} s^{-1}) from the mixed side to the stratified side by the observed tidal excursion (L_m), considering the depth of the pycnocline (D), the time of the front's excursion (T_m) and the nutrients concentration (C) in the mixed side up to the pycnocline depth during neap tide:

$$Q_m\left(mM\, m^{-1} s^{-1}\right) = \left(\frac{L_m}{T_m}\right) \cdot D\, C \quad \text{(Eq. 2)}$$

Given that frontal positions during neap tide present more than one position, a theoretical frontal position for neap tide was estimated with the Simpson and Hunter model (Simpson and Hunter, 1974) to be compared with the observed frontal positions. Then, the theoretical distance of the front was calculated as the average distance between front positions during spring and neap tide. The theoretical front's depth during neap tide (H_{nt}) was calculated from depth-average tidal current amplitude (U_{nt} for neap tide and U_{st} for spring tide) and the observed depth of the frontal position during spring tide (H_{st}) (Equation 3).

$$H_{nt} = H_{st} \cdot \left(\frac{U_{nt}}{U_{st}} \right) \quad \text{(Eq. 3)}$$

The Pingree model (Pingree, 1979; Mann and Lazier, 1996) was applied to estimate the nutrients flux (Q_e: mg m^2 s^{-1}) across the frontal area due to the eddies (Equation 4).

$$Q_e\left(mg\ m^2 s^{-1}\right) = \gamma \left(g \cdot \Delta \rho \frac{D}{\rho_0} \right)^{1/2} D \cdot \Delta C \quad \text{(Eq. 4)}$$

where ΔC and Δρ are the differences in nutrient concentration and density, respectively, across the front, γ is a constant and is equal to 0.0055, g is the gravity acceleration, ρ0 is the constant density value and D is the depth (m). This model was applied to spring and neap tide conditions separately, where ΔC and Δρ have different values at each tidal period, considering that the advection time of a water parcel due to eddies is determined by the inertial period, or 1/f, of an eddy (Pingree et al., 1979) which is smaller than the spring – neap tide time period.

5.7 Chlorophyll *a*

Chl-*a* concentrations were determined by filtering 500 ml of seawater onto 25 mm Whatman GF/F filters that were kept frozen on board at -80ºC until analysis. Pigments extractions were done on board with 90% acetone and fluorescence was measured using a Turner Designs 10 AU fluorometer, following Parsons et al. (1984). Discrete samples of Chl-*a* analysis were used to calibrate the fluorescence sensor by linear regression (Equation 5).

$$[Chl\ a] = 0.61 \cdot F + 0.3;\ R^2 = 0.69\ ;\ n = 38 \quad \text{(Eq. 5)}$$

where F is fluorescence (Relative Fluorescence Units or RFU).

5.7 Plankton

Microplankton (i.e. diatoms, dinoflagellates and ciliates >20 µm) was identified to the lowest possible taxonomic level using a Zeiss Axiovert100 microscope. Cell abundance (cell L^{-1}) was determined using an inverted microscope according to the procedures described by Utermöhl (1958). Subsamples of 50 ml were settled for 24 h in a composite sedimentation chamber prior to counting. The whole chamber bottom was scanned at 20X and higher resolution cells enumerations were made by transects at 40X.

To analyze the cell abundances of organisms smaller than 20 µm, an EPICS® ALTRA™ flow cytometer was used and cytograms were analysed with Beckman Coulter® Expo32 v1.2b software. Nanophytoplankton (2 – 20 µm), picophytoplakton (0.2 – 2 µm) and cyanobacteria cells densities were determined following Tremblay et al. (2009). Heterotrophic bacteria were counted according to the procedures of Belzile et al. (2008).

5.8 Cell carbon content

Picoeukaryotes and bacteria were converted to carbon content using directly a carbon conversion factor depending on cells densities, according to Zubkov et al. 2000, using 12 fg C $cell^{-1}$ for bacteria and 1.5 pg C $cell^{-1}$ for picophytoplankton.

For the other groups, (microplankton, nanoeukaryotes and cyanobacteria) their average biovolume was first calculated and then transformed to carbon content. Biovolume estimates of microplankton groups were made from linear dimensions following the geometric shapes proposed by Hillebrand et al. (1999), analyzing images taken from an

Olympus BX51 microscope equipped with an Image Pro-Plus 5.1 software and camera (Olympus DP70). At least 15 randomly selected cells were measured for each taxa.

Cell carbon content of microphytoplankton groups was calculated following Menden-Deuer and Lessard (2000), considering the parameters a=0.288 and b=0.881 for diatoms and a= 0.216 and b=0.939 for dinoflagellates (autotrophs and heterotrophs). Cell carbon content of ciliates was calculated using the carbon conversion factor of 0.19 pg C µm $^{-3}$ from Børsheim and Bratbak (1987).

Nanophytoplankton average biovolume was computed according to Belzile and Gosselin (2015) and the carbon content was calculated following Tarran et al. (2006), using a conversion factor of 0.22 pg C µm^{-3}.

Finally, the average biovolume and the carbon conversion factor (226 fg C µm ^{3}) for cyanobacteria was estimated following Bertilsson et al. (2003).

5.9 Physiological state of phytoplankton

The cells stress produced by light extreme conditions and nutrient limitation can be evaluated by their fluorescence response (Maxwell and Johnson, 2000; Moore et al., 2006). In this work we evaluated the photosynthetic performance of cells by means of the ratio of variable (F_v) to maximum fluorescence (F_m), the $\boldsymbol{F_v/F_m}$ ratio, the maximum photochemical quantum efficiency of photosystem II (PSII; Misra et al., 2012). We also estimated the energy transfer between closed and open PSII reaction centers, which can be assessed using the connectivity parameter (***p***; Oxborough et al., 2012). These photosynthetic parameters were considered as a proxy of cells physiological state, and measurements were done with a Fast Repetition Rate fluorometer (FRRf; Chelsea Instruments, UK) on 5 ml samples taken directly from the Niskin bottles and kept in the dark for 30 min at sea surface temperature before measurements on board. We used a multiple turnover protocol. The induction of Chl-*a* variable fluorescence was done with 100 flashlets with an interval between flashlets

of 1 µs (total saturation time 200 µs). The interval between acquisitions was 2 s and the relaxation phase was set at 1 ms.

Data processing and figures construction were performed using MatLab ® (R2016a), Gibbs Sea Water routines for MatLab to treat the sea water thermodynamics data (McDougall and Barker, 2011) and, in particular, the maps were made with the mapping toolbox m_map (https://www.eoas.ubc.ca/~rich/map.html). Regression statistics were evaluated with RStudio (3.2.3; R Core Team, 2015).

6. Results and discussion

6.1 Frontal structure

The southern SJG tidal front can be studied both based on vertical density gradients profiles as well as by means of the surface expression of horizontal density gradients.

Density transects across the front (Figure 5) reveal that the frontal boundary can be observed both at the surface and at the bottom of the water column. In this work we focus on the surface expression of the front, considering that it is the most relevant for phytoplankton, given its relation with key environmental variables such as the relative depth of the euphotic zone and the pycnocline, as well as nutrients' availability. To track the same water mass, the surface front position was determined as the position of the 24.9 kg m^{-3} isopycnal at 5m depth, as the shallowest resolved positions of this isopycnal, which was close to the position of the maximum horizontal density gradient on the first transects of the spring and neap tide survey (Figure 5).

The shape of the density structure at the front differs between spring and neap tide. During spring tide, the transition from the mixed to the stratified side is easily recognizable (Figure 5a), varying in density from the latitude -46.58 to the latitude -46.55 ($\Delta\rho$ = 0.2 kg m^{-3}) at surface. In contrast, during neap tide the transition between the mixed to the

stratified side is less sharp and presents two frontal boundaries (Figure 5b), one in which density at surface varies from the latitude -46.58 to the latitude -46.55 ($\Delta\rho$ = 0.1 kg m^{-3}), and a second one varying from the latitude -46.51 to the latitude -46.53 ($\Delta\rho$ = 0.1 kg m^{-3}). In this period, the pycnocline shows a more relaxed vertical density gradient than during spring tide. This is probably because the tidal energy during spring tide can homogenize the deeper layer while the tidal energy during neap tide is weaker and not strong enough to completely mix it.

From spring tide to neap tide, the frontal position moves ~4km northward. It is interesting to note the presence of a second northward frontal expression during neap tide, but this result will be discussed later.

a

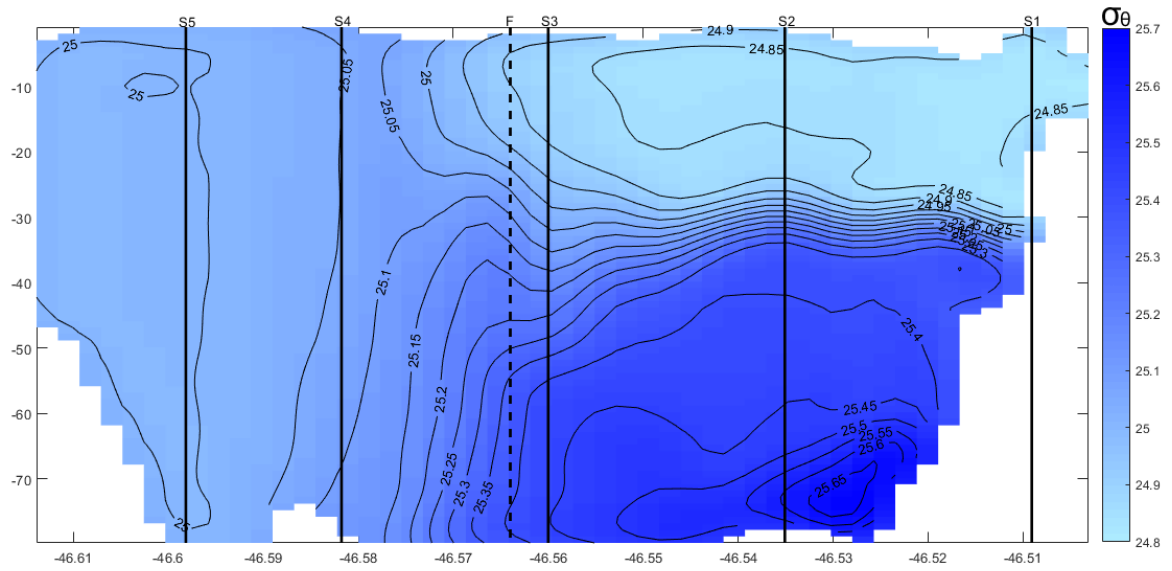

b

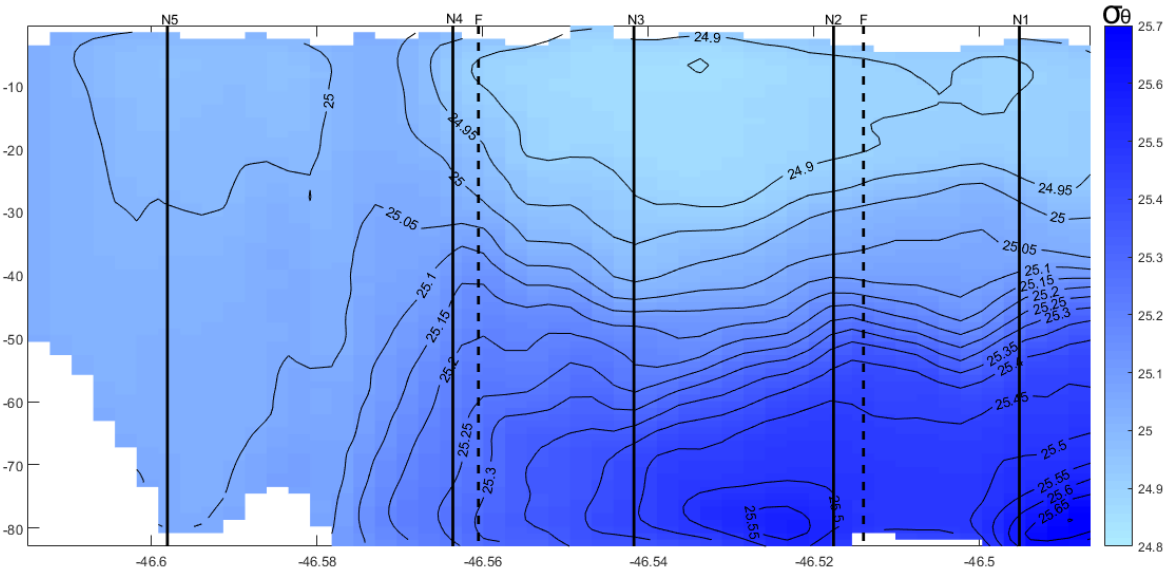

Figure 5: Potential density from the first transects, coincident with the CTD-rosette stations, performed during (a) spring tide and (b) neap tide, showing the rosette stations (black vertical lines) and the frontal positions (black vertical dotted lines).

6.2 Water column profiles

The profiles for the 10 discrete stations performed during February 5 and February 9 further allow us to identify and characterize the vertical structure at both sides of the front and the transitional zone. The stations S3 (Figure 5a) and N4 (Figure 5b) are the closest stations to the frontal interface, so that these stations can be considered as being part of the limit between the stratified side and the mixed side of the front.

The rosette CTD density profiles were further used to calculate the Brunt–Väisälä frequency ($\mathcal{N}^2$) (Figure 6). This model shows that Station S3 had intermediate $\mathcal{N}^2$ values while stations S1 (during spring tide), N1 and N3 (during neap tide) were well stratified, with maximum $\mathcal{N}^2$ at around 40 m or slightly above that depth.

The euphotic depth Z_{eu} was estimated for those stations sampled during daytime (i.e., before 19h –S3, N1, N2, N3, N4, N5). In these stations, Z_{eu} reaches 30 – 40m, which is almost the same depth as the pycnocline depth (Figure 7). This is important because the upper mixed layer determines the depth at which phytoplankton cells are vertically transported from the surface. In this case, the pycnocline depth allows cells to remain in the euphotic zone, providing adequate physical conditions for their growth and biomass accumulation according to the Sverdrup´s model (Sverdrup, 1953).

The maximum values of Chl-*a* were found at ~20m at the stratified stations N1, N2 and N3 during neap tide, with values of Chl-*a* around 0.6 – 0.7 mg Chl-*a* m^{-3}. Stations S2, S4, S5 (during spring tide) and N5 (during neap tide) presented a well-mixed water column, or without any marked pycnocline. Minimal concentrations of Chl-*a* were found at these stations, with values below 0.4 mg Chl-*a* m^{-3}.

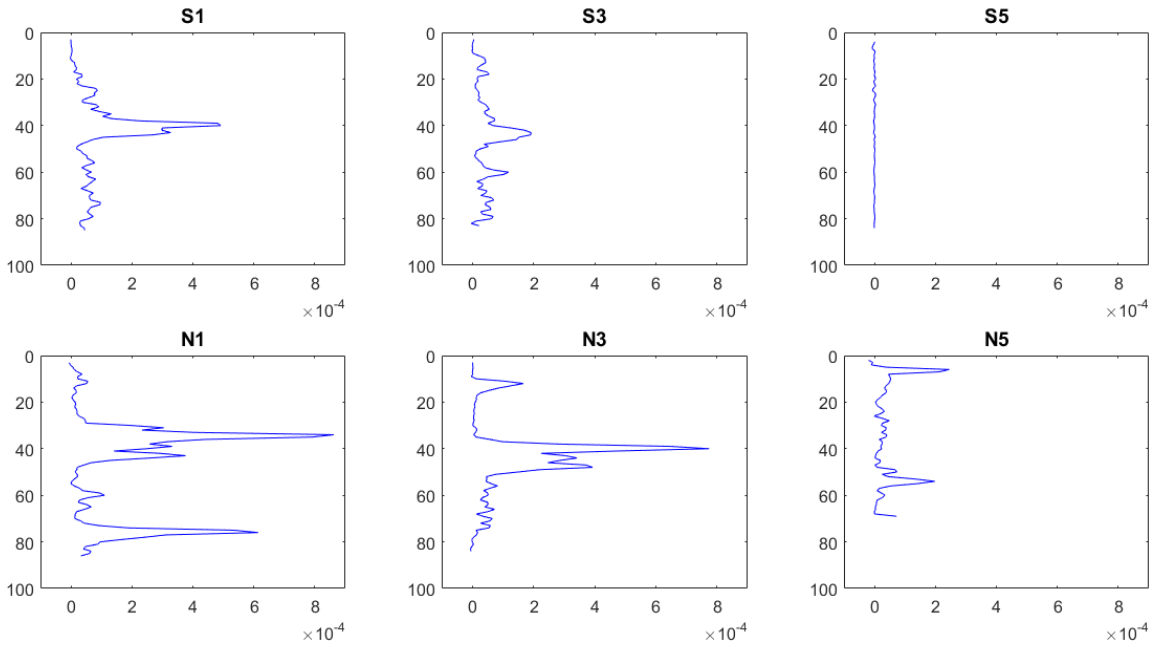

Figure 6: Brunt-Väisälä frequency ($\mathcal{N}^2$) at the discrete, rosette-CTD-sampled stations. The upper row shows the station profiles sampled during spring tide and the second row corresponds to the stations sampled during neap tide. The stations are organized from the stratified side (S1 and N1) to the mixed side (S5 and N5).

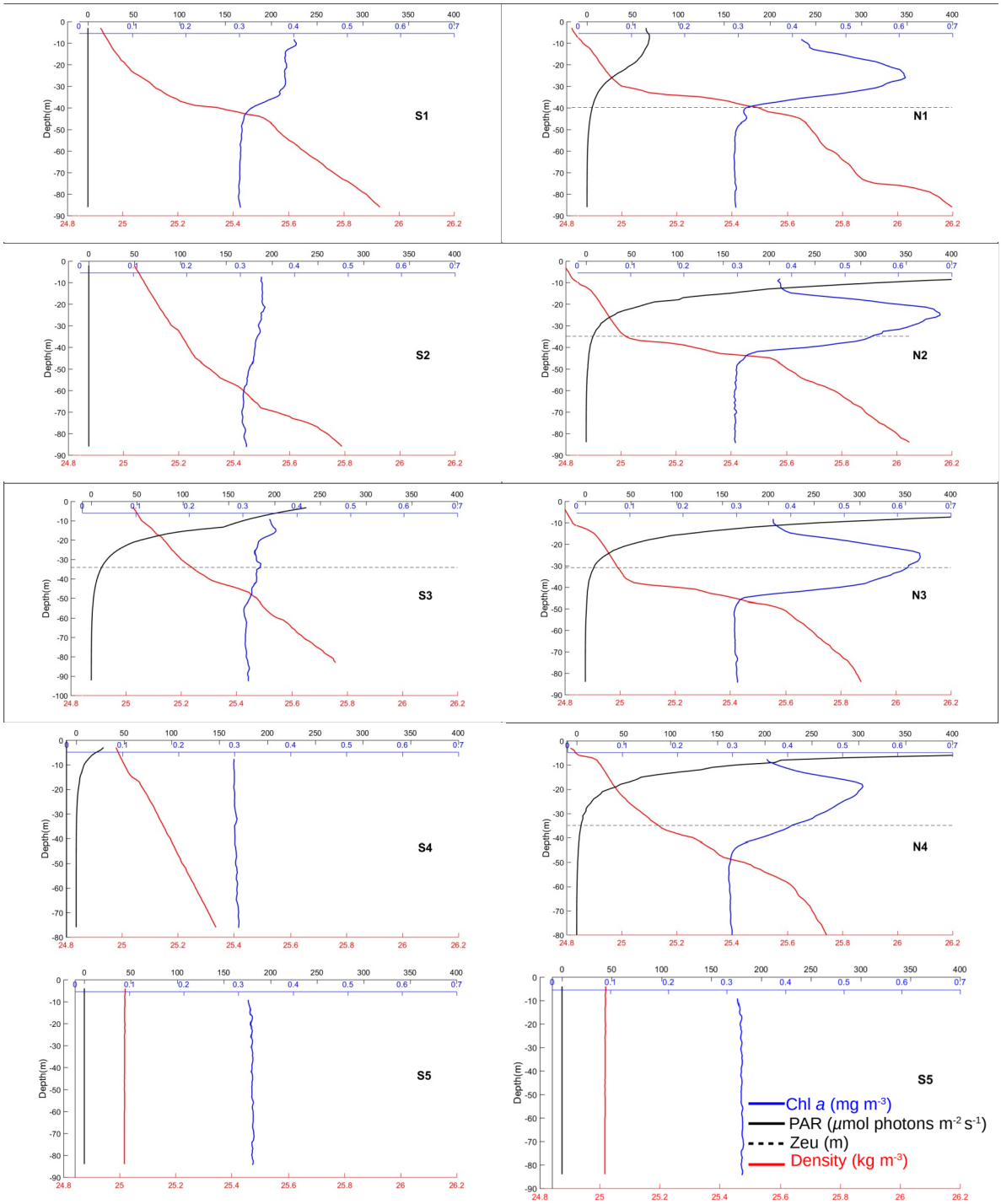

Figure 7: Chl-*a* concentrations (blue line), PAR (black line), Z_{eu} (black dotted line), density (red line) vertical profiles. Left and right columns present stations sampled during spring and neap tide, respectively.

The surface expression of the front (Figure 8) allows the comparison between bathymetry and surface density gradients. During spring tide (Figure 8a), surface density patterns and the frontal positions seem to follow the same semi-circular shape as that the bathymetry does, almost following the 90 m isobath. The shallowest zone (less than 80 m) is coincident with the densest water masses while the deeper zone presents, at the surface, the less dense water masses. This density distribution is as expected, because the deeper depths allow the stratification of the water column, separating the less dense waters in the upper mixed layer from the more dense water masses in the bottom layer by the pycnocline. By contrast, the shallowest zones present a well-mixed water column, where the density is almost the same from the bottom to the surface because of vertical mixing. Supporting this idea, the frontal position during spring tide is close to station S3 (Figure 5a). Northwards of it, the stratified zone is evident (station S1), with σ_θ values in the surface layer of ~24,85, and in the deeper layer, ~25.6. The well-mixed zone (station S5), shows almost the same density values of ~25 over the entire water column (Figure 7).

During neap tide front positions are not consistent with topography (Figure 8b). The western front follows the ~90 m isobath in a semi-circular shape, while the eastern front with the same semi-circular shape follows a depth gradient, from ~65 m to 85 m.

a

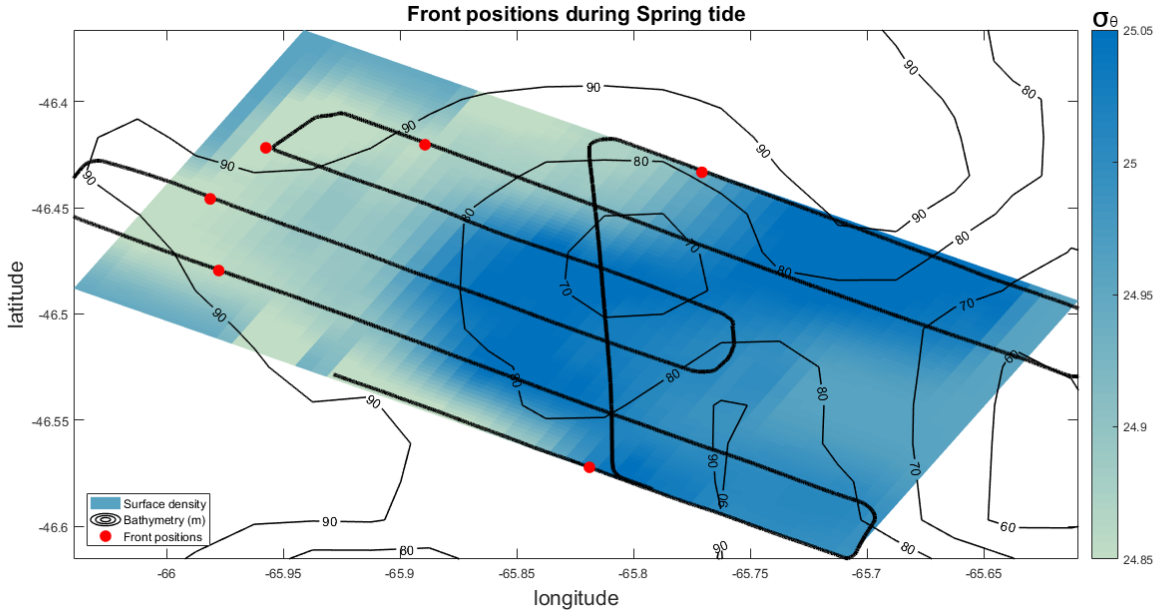

b

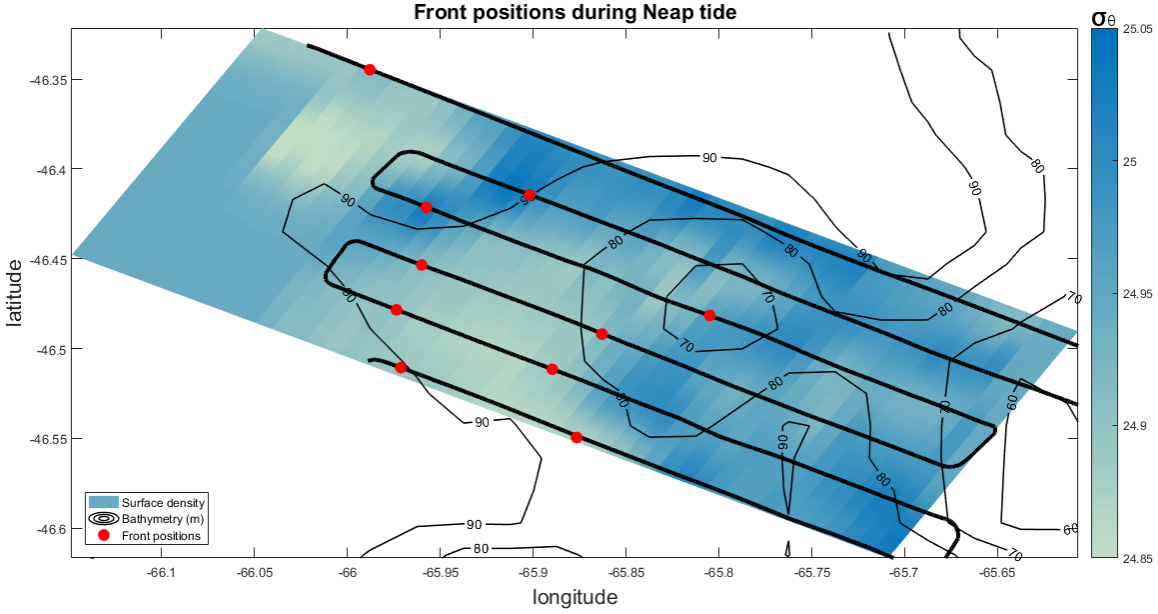

Figure 8: Frontal positions in the SJG during summer 2014 (in red points) plotted over the bathymetry lines. The color represents the average potential density between 3 and 10 m during a) spring tide and b) neap tide.

6.3 Presence of eddies in the frontal zone

To gain more information about the frontal positions we plotted the results obtained from our estimations based on horizontal density gradient over a sea-surface temperature (SST) image (Figure 9) obtained from MODIS-Aqua, from February 4 to February 10 every day at around 15h, local time (from NASA ocean color web page: http://oceancolor.gsfc.nasa.gov). Nevertheless, the less cloudy image was used, corresponding to February 10.

The SST image showed several surface meanders. At the surface, from the longitude -66.2 to -65.9, and between the latitude -46.6 and -46.5, it was evident the horizontal water mass intrusion. In a tongue shape structure, this intrusion is carrying warmer waters, with 15 – 15.5°C (and therefore less dense waters) well distinguishable from the surrounding colder waters with 13.5 – 14°C. This structure is reminiscent of baroclinic instability, and the matched frontal positions estimated with the ROTV density profiles. The baroclinic instabilities are mesoscale features generated by the potential energy difference across the front; they produce eddies-like structures (Mann and Lazier, 1996). It is well known that frontal boundaries are not stable structures and may be altered by the presence of eddies (Pingree 1979). These mesoscale features can remain for a few days and influence the exchange of nutrients and organisms across the frontal region (Pingree et al., 1979).

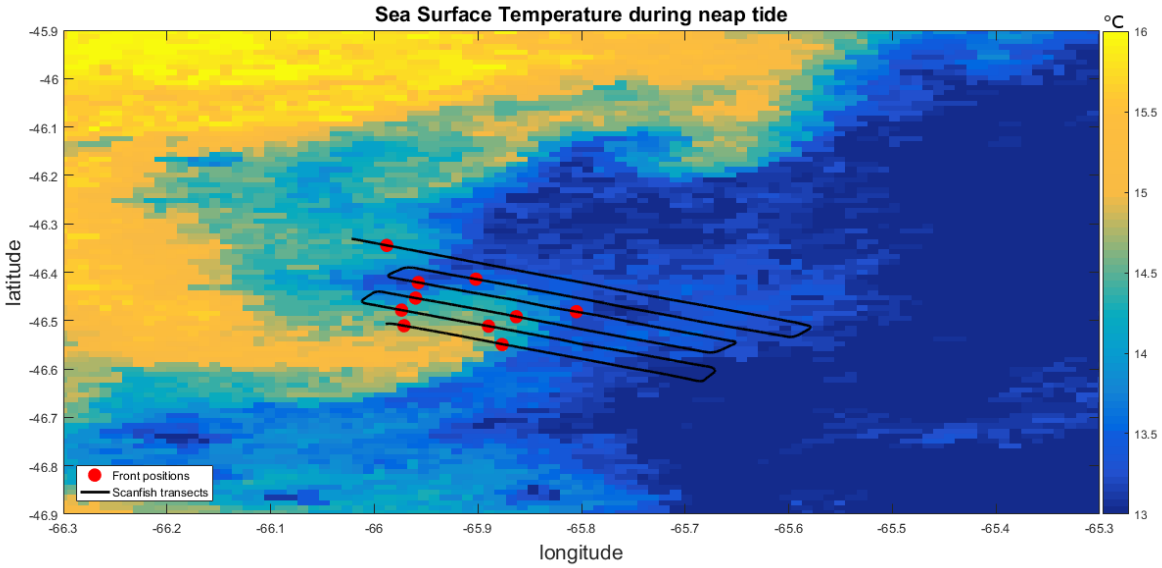

Figure 9: Satellite image of SST (ºC) with front positions (red dots) on the transects.

6.4 Bathymetry and the front position

The bathymetry in the frontal zone of the southern SJG front is complex. In general, it is expected that a tidal front may act as a boundary, separating deep stratified from well-mixed shallow waters (Loder and Platt, 1985). However, there are two deep zones in the south of the SJG divised by an elevation located between the longitudes -65.8 and -65.5 (Glembocki et al., 2015). This feature acts to extend the frontal zone from the inshore to offshore waters. The combination of bathymetry, tidal current amplitudes and the Simpson and Hunter (1974) model allows us to estimate the depth at which the frontal interface should be located over a spring-neap tidal cycle. Figure 10 presents the depth range at which the frontal interface is during spring tide (from 91 m to 83 m) in white lines, and the depth range at which the frontal interface is expected to be found according to Simpson and Hunter (1974) parameter (from 58 m to 63 m). As expected, the tidal positions during neap tide are in shallower waters because the tidal energy is weaker than during spring tide. Frontal positions during spring tide, are expected to be spaced from the frontal positions

during neap tide over an average of 21 km, which is much larger than the average observed (4km), showing that the front position variability was controlled by the mesoscale activity rather than by tidal energy variability.

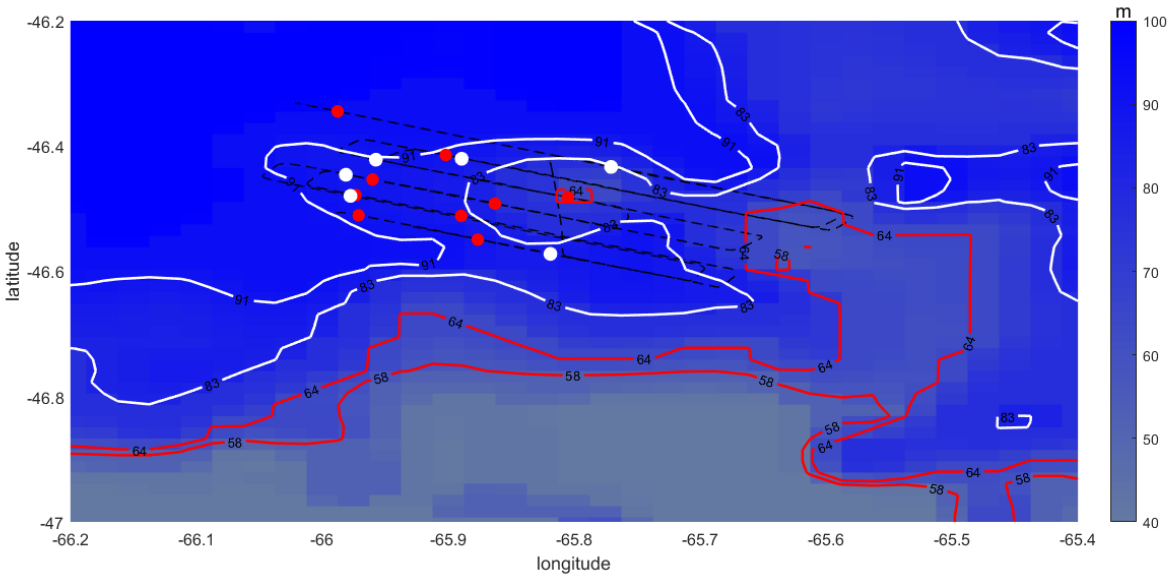

Figure 10: Color map of the bathymetry. White lines are the depth range (91 - 83m) of the observed frontal positions during spring tide. Red lines are the expected depth range (58 - 64m) of the frontal positions during neap tide according to the Simpson and Hunter (1984) parameter. White and red points represent the front position during the spring and neap tide period respectively.

6.5 The effect of tides and eddies on nutrients' distribution

The models of Loder and Platt (1985; equation 2, table 1) and of Pingree (1979; equation 4, table 2) were used to estimate the nutrient fluxes due to tidal and mesoscale variability respectively.

Our calculations show that the SJG undergoes a horizontal displacement similar to that of the Ushant and the Georges Bank fronts (Loder and Platt, 1985). Nutrients (nitrates + nitrites) are supplied at an average rate of 0.45 mg m^{-1} s^{-1} per unit length of front, which is

larger than in other environments (Loder and Platt, 1985). However, one of the limitations of this model is that it does not consider structures such as the observed baroclinic instabilities, which result in eddies's formation (Mann and Lazier, 1996). In frontal zones, these features can be observed at the surface as meander shapes (Figure 9). They are important structures of the front because of their duration (several days) and, at the biological level, eddies participate in the exchange of nutrients and microorganisms across the frontal boundaries (Pingree et al., 1979; Pingree, 1979; Talley et al., 2011).

	Ushant Front	**Georges Bank**	**SJG Front**
L_m (m)	4000	5000	4000
D (m)	20	20	40
C (mg m^{-3})	2	2	3.65
T_m (days)	15	27	15
Q_m (mg m^{-1} s^{-1})	0.12	0,26	**0,45**

Table 1: Results of the model of Loder and Platt (1985) comparing nutrient fluxes at three tidal frontal zones. L_m: displacement of the front between spring and neap tide (m); D: pycnocline depth; C: Nutrients concentration in the upper mixed layer during spring tide on the mixed side; T_m: tidal cycle; Q_m: nutrient flux.

For this reason, the model of Pingree (1979) was applied (Table 2) to estimate Q_e, the nutrient fluxes (mg m^{-1} s^{-1}) resulting from the presence of eddies. In the SJG the depth of the pycnocline is twice deeper than at Ushant front and Georges Bank, but the density difference across the front is smaller.

Comparing the ΔC, here defined as the difference in nutrients concentrations between the stratified and the mixed side across the front, the highest value is found in the SJG during neap tide (Table 2). Moreover, nutrient flux Q_e in SJG during this tidal period is the

highest of the three environements, but it is the smallest during spring tide (Q_e = 0.031mg $m^{-1} s^{-1}$).

	Ushant front	**Georges Bank**	**SJG (spring tide)**	**SJG (neap tide)**
D (m)	20	20	40	40
$\Delta\rho/\rho_0$	6.7 x10^{-4}	10^{-3}	5.2 x10^{-5}	1.06 x10^{-4}
ΔC (mg m^{-3})	2	0.67	1.03	3.05
γ	0.0055	0.01	0.0055	0.0055
Q_e (mg m^{-1} s^{-1})	0.08	0.06	**0.031**	**0.13**

Table 2: Pingree (1979) model comparing three tidal frontal zones. D: Pycnocline depth; $\Delta\rho/\rho_0$: density difference across the frontal interface; ΔC: nutrients concentration difference across the frontal interface; γ: Green (1970) constant; Q_e:nutrient flux.

6.6 Inorganic nutrients availability and POM distribution

As commonly accepted, in marine coastal waters nitrogen is the main limiting nutrient for phytoplankton productivity (Townsend and Pettigrew, 1997). The pycnocline might act as a vertical boundary to the nutrients supply from the deep waters to the euphotic zone, while the frontal interface is a horizontal boundary limiting the exchange between well-mixed waters and stratified waters.

In this study, inorganic nutrients availability in the upper mixed layer has been analyzed by the estimation of the horizontal fluxes (i.e. the above described Loder and Platt and Pingree models). Also, the inorganic nutrients availability to phytoplankton has been studied by discrete concentrations measures in the euphotic layer (Figure 11a). We also contrasted different inorganic nutrient concentrations as ratios, considering the Redfield ratio, and they were related to the stratification level, which were measured by the Brunt-Väisälä frequency $\mathcal{N}^2$ (Figure 11b).

The above-mentioned models were used to explain the potential supply of inorganic nutrients to the upper mixed layer, whereas discrete values and ratios were used to evaluate the potential nutrient limitation to phytoplankton productivity. According to Redfield (1934), under nutrient balanced conditions the atomic N:P ratio is around 16, and a decrease of this value, as we can observe in the figure 11b at all stations, represents N-limiting conditions; in contrast, an increase would represent P-limiting conditions (Geider and La Roche., 2002).

Moreover, a proxy for the nutritional quality of organic matter is the content of POM (particulate organic carbon, POC, and particulate organic nitrogen, PON) and more precisely the POC:PON ratio (commonly called C:N ratio) (Townsend and Thomas, 2002). Phytoplankton organic matter is usually high in proteins, carbohydrates and lipids content (Copin-Montegut and CopinMontegut, 1983), and presents values of the C:N ratio lower than detritus organic matter. A Redfield C:N ratio of 6.6 corresponds to the balanced organic matter but it can reach values from 3.8 to 12.5 (Geider and La Roche, 2002). The greater variability of this ratio is related to the depth, reaching values between 8 and >15 in deep waters while in the surface layer, the C:N ratio may range 5 to 8 (Copin-Montegut and CopinMontegut, 1983).

Low C:N ratios represent a nitrogen enrichment of the organic matter, which is normally considered as high-quality food available for consumers (Townsend and Thomas, 2002). The tendency to increase this ratio can be explained by the increase of detritus or the heterotrophic organisms (Townsend and Thomas 2002), suggesting a more rapid utilization of proteins than carbohydrates (Copin-Montegut and CopinMontegut, 1983).

Dissolved inorganic nitrogen (nitrates + nitrites) concentrations registered above the pycnocline in the SJG during spring are about 0.5 - 2 µM (Akselman, 1996) and during autumn are 1.8 µM (Krock et al., 2015). However there are no previous records about the inorganic nitrate + nitrite concentrations during summer.

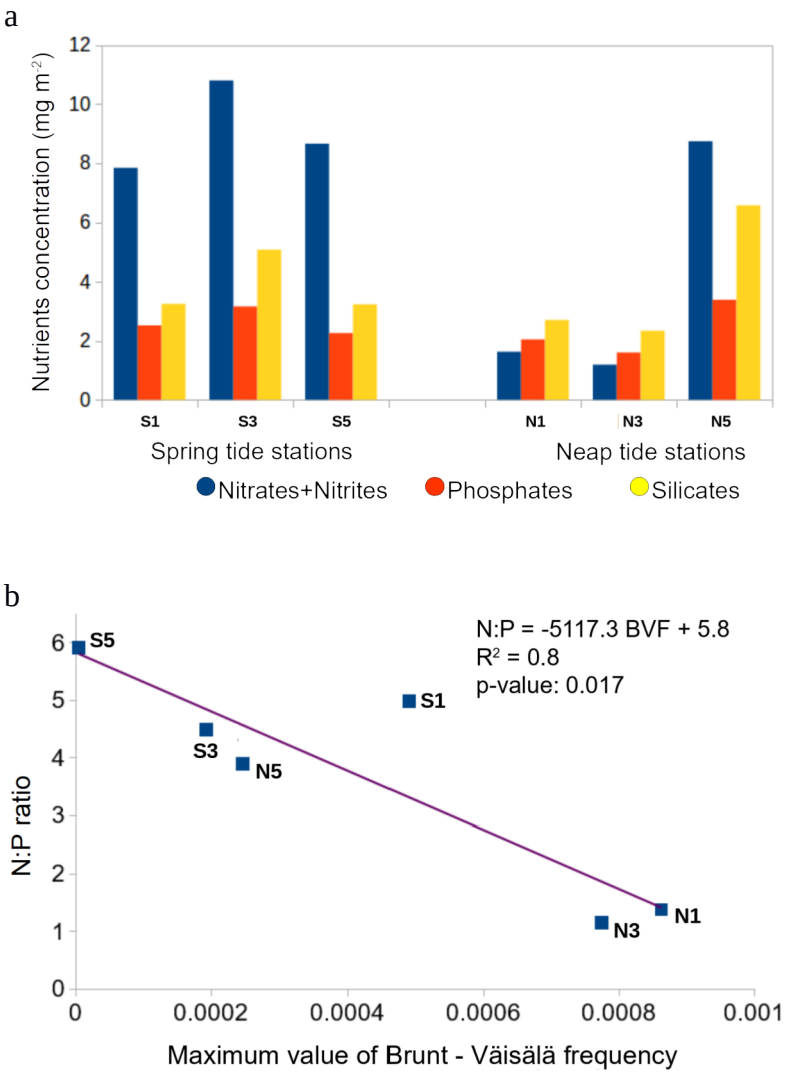

Figure 11: a) trapezoidal integration of nutrients concentration in the upper mixed layer (mg m^{-2}) during spring tide (S1, S3, S5) and neap tide (N1, N3, N5). Blue, orange and yellow bars are nitrates+nitrites, phosphates and silicates, respectively. b) Linear regression of the N:P ratio as a function of the maximum value of Brunt-Väisälä frequency at each station.

The trapezoidal integration of nutrient concentrations (nitrates+nitrites, phosphates and silicates) above the pycnocline are presented in the figure 11a. The models approach allow us to understand if the discrete nutrient concentrations in the upper mixed layer are being advected by horizontal movements or by vertical fluxes. The results showed in this figure, it is noteworthy that the stations N1 and N3, during neap tide, present the minimal nitrogen availability. Those stations were the most stratified ones and this nutrients' limitation is in line with the presence of the pycnocline, which was separating the deeper nutrients-rich waters from the upper nutrients-poor layer. These observations agree with the figure 11b, where the N:P ratio, established from the nutrients concentration in molecular forms at the maximum Chl-*a* depth, was plotted in function of the stratification in the water column. The largest $\mathcal{N}^2$ was found at N1 and N3 stations showing that these stations were the most stratified and presented the lowest N:P ratio. Considering that phytoplankton cells are able to uptake dissolved inorganic nitrogen at external concentrations as low as 0.2 – 0.3 µM, where the nitrate is the most abundant form of inorganic N (Reynolds, 2006), the minimal inorganic nitrogen concentrations found at N1 and N3 were not below the inorganic N concentration to limit the phytoplankton uptake in the southern SJG frontal zone.

Nevertheless, the models used here suggest a high horizontal flux of nutrients (Tables 1 and 2), however discrete concentration are not so high, so that perhaps nutrients were being horizontally advected away from the sampled zone or were consumed by phytoplankton cells.

Stations S5 and S3 were in the most mixed waters in this study, as shown by the values of $\mathcal{N}^2$. S5 was the only station with N:P close to 6, which could be a result of the water column being well mixed during the entire fortnightly tidal cycle. This result is similar to findings from the North Atlantic during winter, when the water column was well mixed (Geider and LaRoche, 2002).

By contrast, while the Pingree's model showed the smallest nutrient flux during spring tide (Table 2), Figure 11a showed that stations sampled during spring tide (S1, S3 and S5) presented the highest nutrient concentrations. This could be a consequence of an accumulation effect, and in this case we could hypothesize three possible scenarios, which we will additionally relate to the planktonic food web:

The first scenario is a minimal uptake of inorganic nutrients. This could happen if photosynthetic organisms were under a high grazing pressure or if they were in bad physiological shape. The grazing pressure can be discriminated from the bad physiological shape considering that phytoplankton cells are the intermediate link between inorganic nutrients and heterotrophic groups. As a consequence, the heterotrophic groups would be very important, indicating a fast energy transfer to superior levels of the trophic web and the C:N ratio will present values around or less than 6. And if the phytoplankton is in bad shape, the heterotrophic community wont be important and the parameters F_v/F_m and p would present very low values.

The second scenario corresponds to a physical accumulation effect, where the energy transfer between the different food web levels was slow, there would be an accumulation of bacteria and the productivity would be enhanced by recycling in the microbial loop. As a consequence, the degradation of organic matter would be very important and the C:N ratio could reach values over 7 (Caron et al., 1995).

The C:N ratio as a function of the stratification is presented in Figure 12. As it can be seen, the ratio was in general < 7 at all stations, which was indicative of a high-quality organic matter. The main characteristic of this regression is the negative slope, showing a decrease of the C:N ratio as stratification increases (larger $\mathcal{N}^2$). When C and N are actively incorporated into nucleic acids, amino acids or proteins, cells C:N ratio can vary from 2.6 – 3.8 (Geider and La Roche, 2002). At weak stratification, stations S5 and S3, present the highest C:N ratio, close to 7, where there could be an influence of the degraded organic matter resuspended from the bottom to the surface due to vertical mixing. At strong

stratification, stations N3 and N1 present the minimal C:N ratio, around 2 - 4, indicating that the organic matter was of better quality. According to the models, these stations received strong inorganic nutrients' fluxes although they were not in high concentrations. Therefore, we hypothesize that at these stations the inorganic nutrients were being quickly assimilated and transformed into new organic matter.

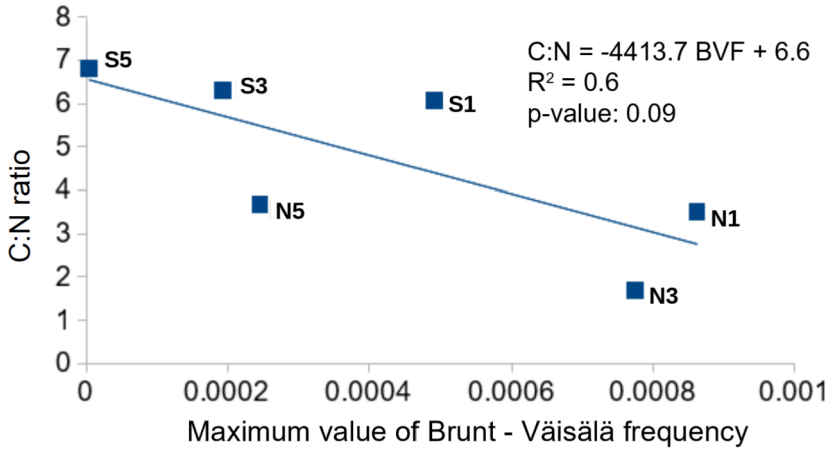

Figure 12: C:N ratio as a function of the maximum value of Brunt - Väisälä frequency at each station.

6.7 Plankton biomass and composition

To compare the biomass of the autotrophic community during both tidal periods, we plotted the Chl-*a* concentration, obtained from the fluorescence sensor attached to the ROTV along the first transect (Figure 13). Similarly to other systems, maximum values were found during neap tide (Cloern, 1996; Landeira et al., 2014). In our observations, the maximum values measured for Chl-*a* were 1.2 - 1.3 mg m^{-3}, which were lower than previous results from the southern SJG frontal zone during summer, when values were around 2 - 2.3 mg Chl-*a* m^{-3} (Cucchi-Colleoni and Carreto, 2001; Fernández et al., 2005) During both tidal periods, the highest Chl-*a* concentrations were limited between the

pycnocline and the surface, reaching the maximum values around 10 - 20 m depth. Maximum Chl-*a* concentrations were found enclosed between the two frontal boundaries previously described during neap tide. During spring tide, Chl-*a* concentrations were lower, with values below 0.7 mg Chl-*a* m^{-3}. The maximum values on the stratified side of the front were measured at station S1.

a

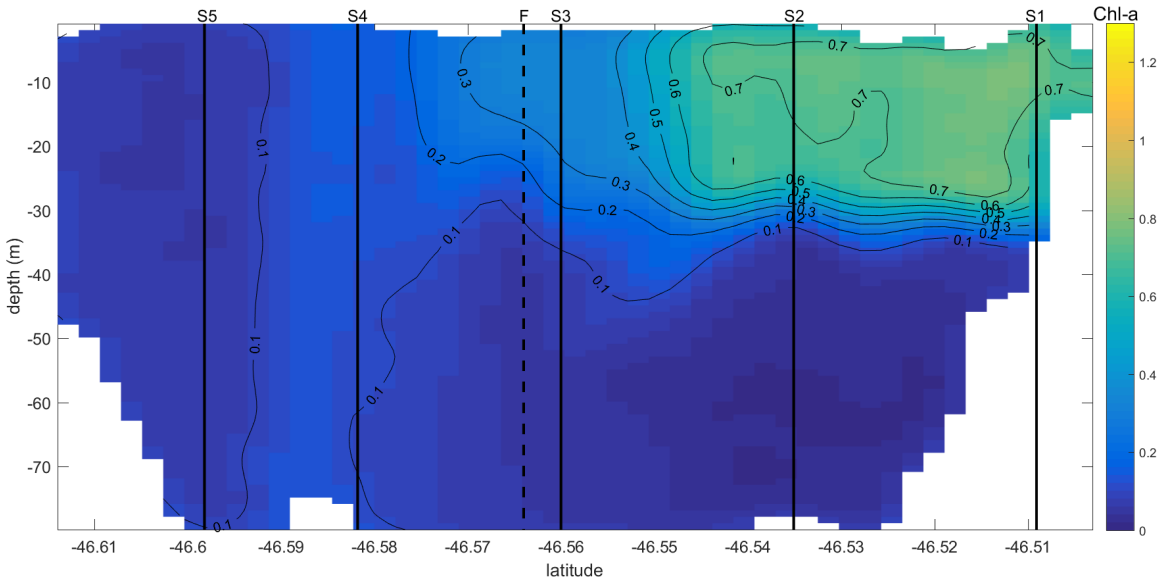

b

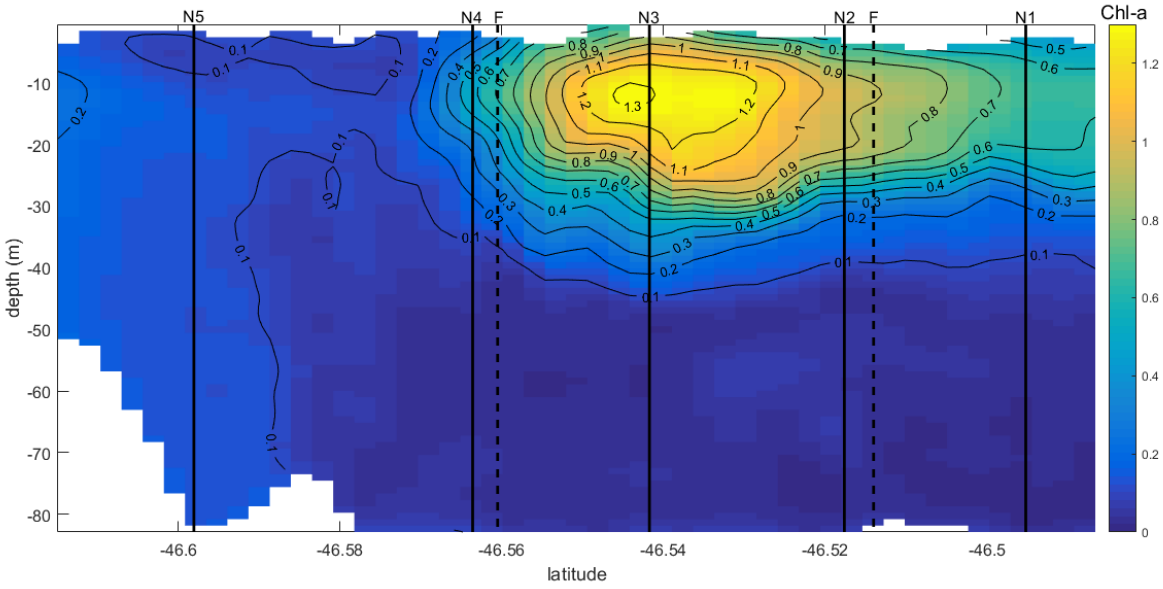

Figure 13: Chlorophyll *a* concentration in the first transect during (a) spring and (b) neap tide, respectively. Dotted vertical lines represent the frontal positions. Filled vertical lines are stations sampled with the rosette.

In order to understand the carbon contribution of the different microbial groups at each station, we separated the biomass of both phytoplankton (Figure 14a) and heterotrophic organisms (Figure 14b). Following Olenina et al. (2006), dinoflagellates were grouped in two categories: autotrophs, corresponding to *Ceratium lineatum*, *Prorocentrum micans*, *Alexandrium* sp.; and heterotrophs plus mixotrophs, including to *Gymnodinium* sp, *Dynophisis acuminata*, *Protoperidinium* sp, *Gyrodinium* sp. In terms of biomass, most of the autotrophic organisms belonged to the nanophytoplankton size class (2 - 20 µm) at almost all stations. However, in station S1 microplanktonic (> 20 µm) dinoflagellates presented the highest carbon contribution. Station S3 shows the maximum contribution of microplanktonic diatoms to total biomass, although they represented only a low percentage. This is noteworthy because S3 was the station closest to the frontal position during spring tide, and as theory predicts, diatoms tend to be dominant in nutrients-rich, turbulent waters (Glibert, 2016).

At stations N1 and N3, in which the highest values of carbon biomass were reached in line with the highest Chl-*a* values from ROTV transects, nanophytoplankton, picophytoplankton and cyanobacteria were the most important groups. In the well mixed station N5 minimal plankton biomass concentration was observed.

Regarding heterotrophic organisms, bacteria were the most important group contributing to total heterotrophic biomass during neap tide, whereas ciliates and dinoflagellates reached also high values during spring tide (Figure 14b) in the stratified side of the front (stations S1 and S3). Even if the stratified side of the front during spring tide (station S1) was characterized by high nutrients' availability (Figure 11a; Figure 20 Annex), there was less autotrophic biomass accumulation, but it is possible to infer the presence of high grazing pressure, considering the high biomass of ciliates and heterotrophic dinoflagellates, again in accordance with the first hypothesized scenario described above.

Stations with minimal heterotrophic biomass concentrations,S5 and N5, were coincident with minimal Chl-*a* concentrations and the well-mixed water conditions.

a

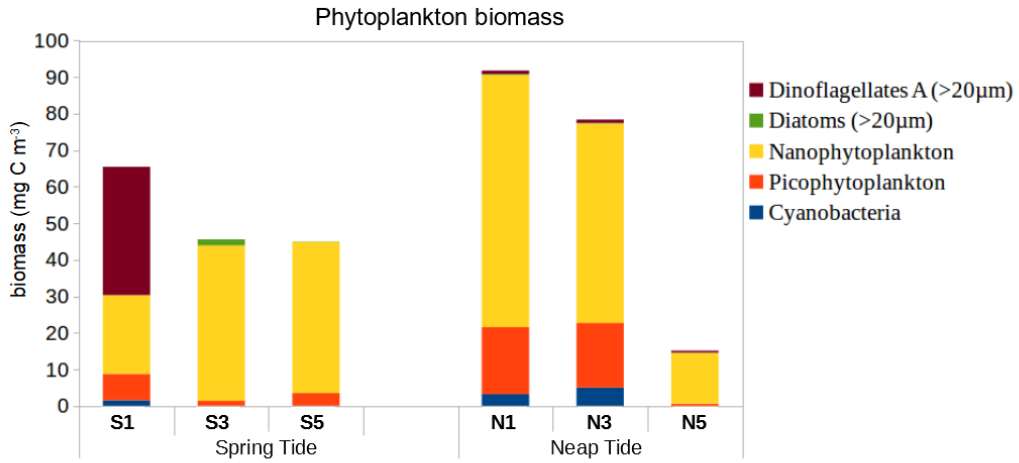

b

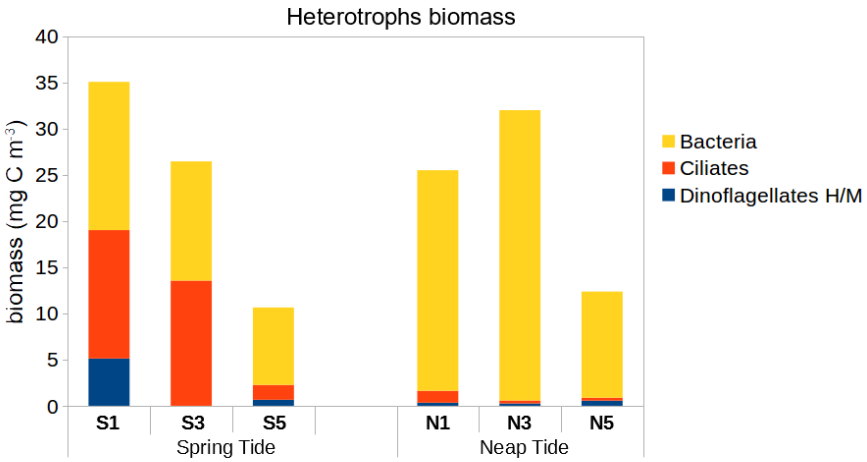

Figure 14: Biomass of phytoplankton (mg C m $^{-3}$) main groups (a) and biomass of main heterotrophic groups (b).

Considering cell densities of autothrophic phytoplankton, cyanobacteria were the most abundant group, followed by pico- and nanoeukaryotes (Figure 15). Stations N1 and N3 presented the highest total cell densities, and a higher contribution of the nano- and

picophytoplankton fractions. The well-mixed stations N5 and S5 and the station S3, in the frontal interface, presented the lowest cell abundances.

Considering the heterotrophic groups, the bacterial community was the most abundant group at all stations (Figure 16b). The highest bacteria cell abundances were found at stations N1 and N3. Regarding the heterotrophic eukaryotic cells (Figure 16a), dinoflagellates were more important than ciliates at all stations but especially at station S1. The highest abundance of ciliates was observed at station S3.

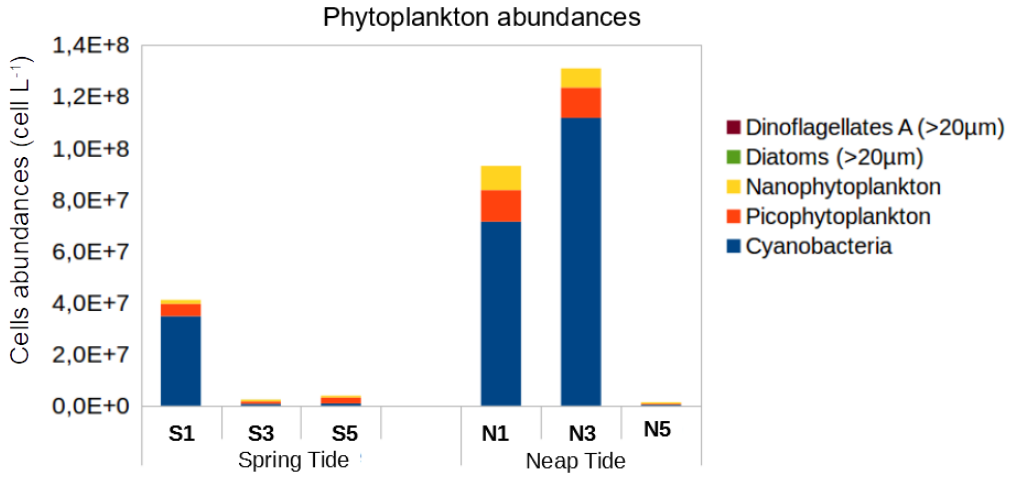

Figure 15: Cells abundances (cells L^{-1}) of the micro-, nano-, picophytoplankton eukaryotes and cyanobacteria.

a

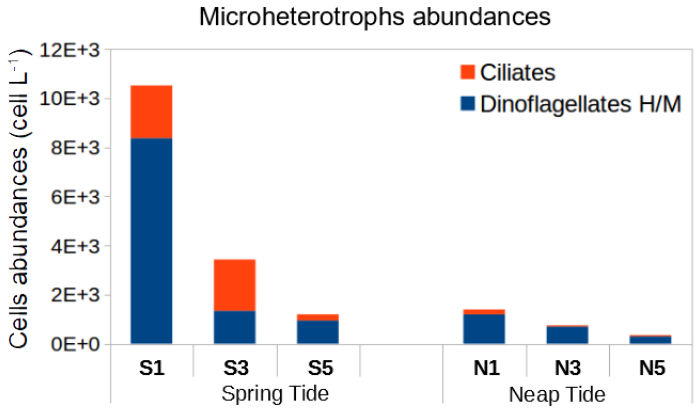

b

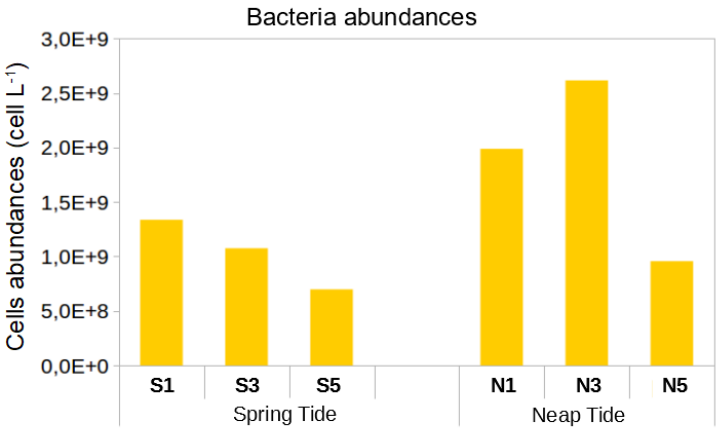

Figure 16: Heterotrophic cells abundances (cells L^{-1}): (a) dinoflagellates, ciliates and (b) bacteria.

6.8 Plankton carbon contribution to the POC pool

To learn about the contribution of the microbial carbon to the particulate organic carbon at the depth of the Chl-*a* maximum, two regressions were made, relating the POC to phytoplankton carbon (Figure 17a) and to heterotrophs+phytoplankton (Figure 17b) biomass, respectively. The intercept of the first regression shows that the POC reached 105 mg C m^{-3} when the contribution of phytoplankton biomass is zero, probably provided by detritus or heterotrophs' carbon biomass. When phytoplankton carbon is added to the heterotrophic carbon, the *y* intercept is reduced from 105 mg C m^{-3} to 94 mg C m^{-3}, indicating that there is a high amount of detritus and probably faecal pellets in the particulate organic matter (Massé-Beaulne et al., 2017). A more precise description of the detritus present in the POC is given when autotrophs and heterotrophs biomass are considered.

In addition, the slopes are different, so that when only phytoplankton biomass is considered, the slope of the regression is larger than the slope of the POC as a function of phytoplankton + heterotrophic biomass. Thus, phytoplankton biomass is more important as a carbon contribution to the particulate organic carbon pool than the rest of the community.

a

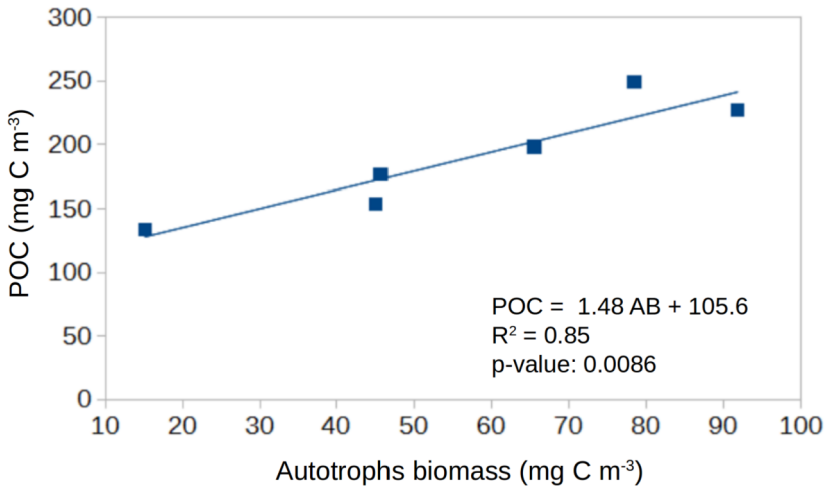

b

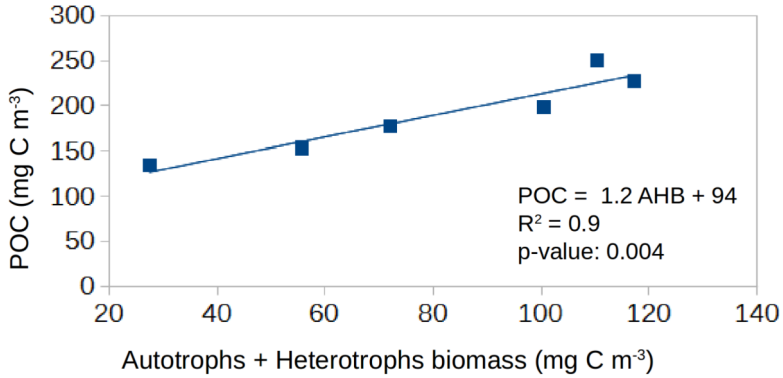

Figure 17: (a) Linear regression between POC vs. autotrophic biomass. (b) POC vs. autotrophs + heterotrophs biomass.

6.9 Physiological state of photosynthetic cells

To understand how the environmental conditions in the frontal zone (i.e., mixed or stratified water column, nutrients availability, euphotic depth) affect the physiological state of the autotrophic assemblages, we studied the photosynthetic quantum yield and the connectivity between reaction centers at two different depths: surface and Chl-*a* maximum depth (Figure 18) to estimate the cells photo-inhibition and their physiological state.

Based on the F_v/F_m ratio (Figure 18a), it is possible to determine that at Chl-*a* maximum depth, cells are in better physiological conditions than at surface, showing a photo-inhibition state at the surface except at station S1.

The *p* parameter shows a pattern similar to that of F_v/F_m, but the best cell conditions (highest *p*) are found at the stations N1 and N3.

Considering that the smallest cells, such as pico-eukaryotes, have a signature of F_v/F_m between 0.3 and 0.4 and that cyanobacteria have a signature between 0.1 and 0.4 (Suggett et al., 2009), we can infer that the cells are photosynthetically active in the natural environmental conditions of the frontal zone. In the well mixed stations S5 and N5, where the cell abundances and biomass were the lowest, the physiological state of the cells is similar to that of the other stations. We hypothesize that although cells are being transported from the surface to the bottom, they are able to adapt their photosynthetic apparatus to the water column average light intensity. Moreover, nutrients do not seem to affect the photosynthetic parameters studied.

Comparing the *p* parameter between spring and neap tide at Chl-a maximum depth, it is observable that during spring tide the connection among the reaction centers is lower than during neap tide. This result agree with the first scenario justifying the minimal uptake of inorganic nutrients during spring tide which is coincident with the highest microheterotrophs abundances, supporting the strong grazing pressure scenario.

a

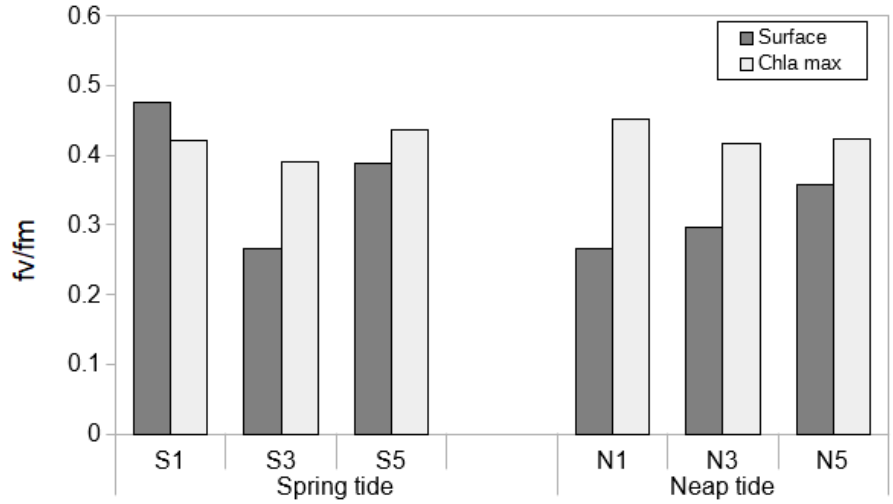

b

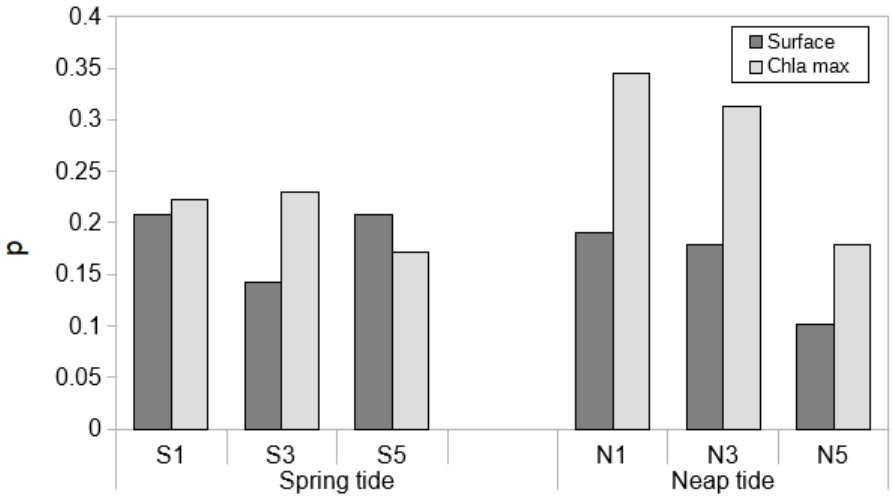

Figure 18: photosynthetic quantum yield of phytoplankton cells at surface (dark bars) and Chl-*a* maximum depth (gray bars). (a) F_v/F_m parameter. (b) *p* parameter.

7. Conclusions

Connecting the above information, the stratification evaluated with the Brunt–Väisälä frequency allows us to separate stations S1, N1, N3 ($\mathcal{N}^2 >= 4 \times 10^{-4}\ s^{-1}$) from stations S3, S5 and N5 ($\mathcal{N}^2 = < 2 \times 10^{-4}\ s^{-1}$). All the well-mixed stations present an important nutrient flux through horizontal transport. Station S3 is particular because it is part of the frontal interface. This station presents high inorganic nitrogen availability but the quality of the organic matter is lower than at the other stations. The main phytoplankton groups, in terms of biomass, are the nanoeukaryotes and microplanktonic diatoms (>20 µm). The main heterotrophic groups, in terms of abundances and biomass, are bacteria and ciliates. All stations present a N:P ratio <16 and, as already described, this represents N-limiting conditions.

Since the horizontal nutrient flux is weak during spring tide, we expected to find a quick uptake by autotrophic organisms, and, consequently, low inorganic nutrients concentration and high phytoplankton cells' densities, which can be expressed in a low C:N ratio. However, station S1 presents high inorganic N concentration above the pycnocline (Figure 11a ~8 mg m^{-2}; Annexe: Figure 20, 2 – 4 µM), and the plankton assemblages show large microphytoplankton cells such as autotrophic dinoflagellates, which have long life cycles and are able to swim searching for their optimal growth conditions, and have a slow growth rate (Glibert, 2016). Nevertheless, this autotrophic community is probably under an important grazing pressure by the mesozooplankton. Gimenez et al., (in press) described a high copepodits and *Ctenocalanus vanus* abundances, and a high young Euphausiid stage (including *Euphausia vallentini*) and *Ctenocalanus vanus* biomass in the frontal area. The dynamics of this trophic food web results in a large amount of detritus, constituted specially by large particles such as faecal pellets or macroagregates. However the high cianobacteria abundances provide probably with relatively high amounts of nitrogenous compounds resulting in a C:N ratios around 7 during summer (Fernández et al., 2008; Massé-Beaulne et

al., 2017). However, these results were obtained in the central region of the Gulf, while the production zone we describe here corresponds to the coastal south-east area. The spatial difference between the frontal zone production at south-east, and the depositional central zone of the SJG, could result from eddies transport or from local production in the center of the Gulf.

On the other hand, stratified stations during neap tide (N1 and N3) were characterized by high nutrient fluxes whereas inorganic nutrients concentrations were low. The assimilation of nutrients by autotrophic organisms is supported by the presence of high cells' densities and high autotrophic and heterotrophic biomass production. This microbial community is very different from that developed during spring tide, because in this case it is characterized by small photosynthetic cells and high bacteria cells density and biomass. These organisms have short life cycles and high growth rates. Glibert (2016) characterize these assemblages, composed by pico-phytoplankton and small flagellates, as having high rates of regenerated production (microbial loop). This agrees with the observed N:P ratio, which is close to 0 when the recycled production fuels the primary production (Towsend and Thomas 2002). Regarding the physiological results, the *p*parameter shows the maximum values at N1 and N3 stations, among 0.3 and 0.4. Considering that cyanobacteria have a signature in natural environments between 0.1 and 0.4 (Suggett et al., 2009) we can conclude that this stations present the optimal conditions of light and nutrients for cianobacteria growth.

8. Conclusion générale

Notre étude montre que la bathymétrie de l'aire frontal du sud du Golfe San Jorge est complexe et la présence d'une diminution marquée de la profondeur dans le sud-est permet d'étendre la surface horizontale du front, loin de la côte sud vers le nord-est. La position du front migre d'environ 4 km sur un cycle de marée morte-eau/vive-eau, une distance bien inférieure à celle prédite par le modèle de Simpson et Hunter (1974) basé sur l'énergie cinétique de la marée et la bathymétrie.

Les analyses des images satellitaires de température dans la surface de la mer ont permis l'observation d'instabilités baroclines qui modifient la structure frontale.

Le transport horizontal de nutriments a été estimé à l'aide de deux modèles : 1) le modèle de Loder et Platt (1985), qui considère les effets de la marée vive-eau/morte-eau sur la disponibilité de nutriments dans la zone stratifié pendant la marée morte, comme consequence de l'approximation de la pycnocline vers la zone cotière; 2) le modèle de Pingree (1979) qui évalue l'influence des tourbillons. Le modèle de Pingree (1979) suggère que le flux de nutriments est plus grand durant la marée morte-eau que lors de la marée vive-eau, ce qui permet le développement d'une accumulation plus grande de biomasse autotrophe.

Les analyses biologiques ont montré que le côté stratifié de la zone frontale est plus variable par rapport aux différents groupes de la communauté du phytoplancton en considérant les effets d'un cycle de marée vive-eau /morte-eau. Le côté stratifié pendant la marée morte-eau permet une accumulation de biomasse majeure, où les groupes les plus importants, contribuant au pool de carbone d'origine autotrophes, sont les cellules plus petites que 20 µm : nano-, picophytoplankton et cyanobactéries, tandis que la biomasse d'origine hétérotrophique est dominée par les bactéries.

Cependant, le côté stratifié pendant la marée de vive-eau présente une grande contribution par les cellules de grande taille comme les dinoflagellés et les micro-

diatomées. À son tour, la biomasse des hétérotrophes est dominée par les grandes cellules comme les ciliés et les dinoflagellés hétérotrophes.

Du côté mélangé les analyses sur l'état physiologique des cellules autotrophes montrent que le mélange vertical permet la photo-acclimatation de l'appareil photosynthétique aux conditions optimales de lumière. Cela suggère que les cellules près de la surface, qui sont probablement photo-inhibées, et les cellules sous la zone photique, qui sont privées de lumière, sont rapidement transportées par les mouvements turbulents verticaux vers les profondeurs où l'irradiance est optimale. Le bonne état physiologique dans le côté mélangé est aussi soutenue par la disponibilité des nutriments.

La figure 19 est un modèle conceptuel montrant la dynamique de la communauté microbienne pendant la marée vive-eau et la marée morte-eau du coté stratifié du front dans la couche de surface. Les flux horizontaux et les concentrations de nutriments sont représentes par des flèches et des boîtes rouges, et la valeur du rapport N:P est indiquée dans les boîtes correspondant aux nutriments. La biomasse du phytoplancton est plus élevée pendant la marée morte-eau et les petites cellules (<20 μm) sont les plus représentatives, due aux conditions de plus forte stratification et, en consequence, la limitation de nutriments. En revanche, la biomasse du phytoplancton pendant la marée vive-eau est en faible concentration et est dominée par les cellules de plus grande taille (>20 μm), ce qui corresponde aux eaux riches en nutriments et plus faible stratification.

La biomasse des cellules hétérotrophes est divisée en deux boîtes de couleurs différentes, une boîte pour les bactéries et une autre pour les cellules eukariotes comme les dinoflagellés et les ciliés. La biomasse des bactéries est plus importante pendant la marée morte-eau que pendant la marée vive-eau, mais l'inverse a été observé pour les ciliés et les dinoflagellés. Encore, l'stratification pendante la marée morte-eau conditionne l'échange verticale avec les eaux profondes, parce que la forte pycnocline joue en rôle de frontière pour la fourniture verticale de nutriments, et la couche isolée de surface mène le développement d'une réseau trophique soutenue par le bouclé microbienne, où les bactéries

son protagonistes. Tandis que pendante la marée vive-eau, la faible pycnocline permet l'échange verticale avec les eaux profondes riches en nutriments et en conséquence, le développement d'une communauté microphytoplanktonique donc une communauté hétérotrophe de plus grande taille, avec mobilité pour chercher les conditions optimales de nourriture malgré l' énergie de turbulence. Ce transfer d'énérgie entre le phytoplancton et les micro et mesohétérotrophes est représente par une flèche noire.

La matière organique pendant la marée morte-eau présente une meilleur qualité nutritionelle que pendant la marée vive-eau, tel qu'observé avec le ratio C:N, en soulignant l'importance des groupes nano et picophytoplanktonique dans la communauté des producteurs primaires marines.

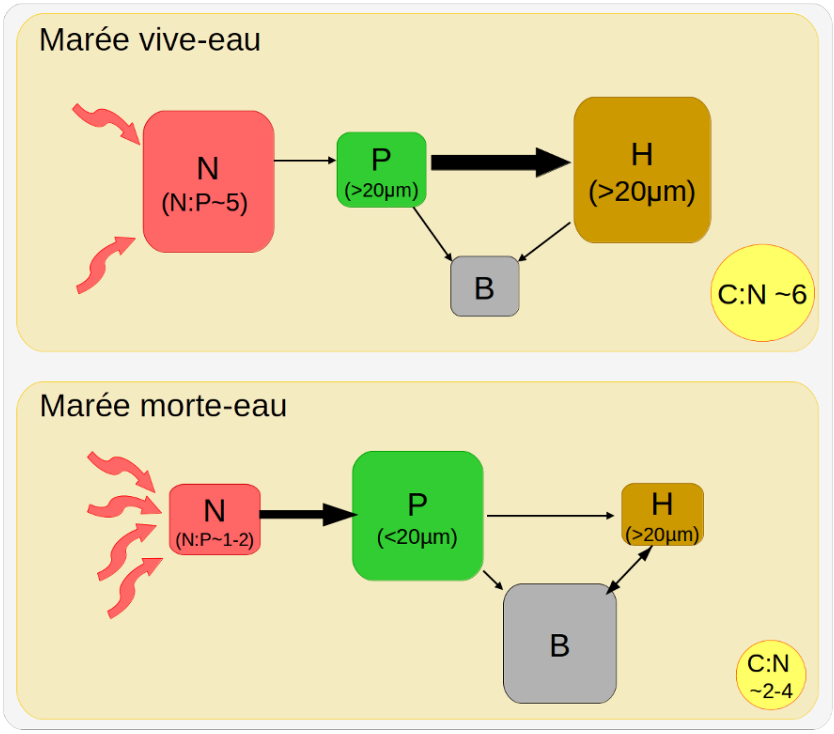

Figure 19: La dynamique de la communauté microbienne du côté stratifié de la zone frontale du sud du GSJ pendant la marée vive-eau et la marée morte-eau. Les flèches rouges représentent les flux horizontaux de nutriments; la taille des boîtes et des flèches noires représent l'importance de la concentration ou du flux. N est la disponibilité des nutriments; P est la biomasse du phytoplancton; H est la biomasse des hétérotrophes; B est la biomasse des bactéries.

Les perspectives de recherche

Comme ces fronts sont très dynamiques, idéalement il faudrait d'abord effectuer un suivi journalier du front sur une période couvrant le cycle complet vive-eau/more-eau. Ensuite, il faudrait investiguer plusieurs cycles de marée au cours d'une même année afin d'estimer la variabilibé intra-annuelle. Il sera intéressant lors d'études futures de suivre les positions de ce front à l'aide des images satellites pendant plusieurs cycles de marée morte-eau / vive-eau interannuelle, afin de filtrer les effects des tourbillons méso-échelle et de faire ainsi ressorit la variabilité associée au cycle de marée vive-eau/morte-eau, ce quei permettrait une meilleure compareaison avec les modèdes théoriques comme Simpson et Hunter (1974). Par ailleur une telle étude permettrait évaluer les interactions entre le cycle de marée vive-eau/ morte-eau, le vent et les phénomènes de meso-échelle. D'ailleurs, une bonne compression du comportement et développement des tourbillons dans le sud du SJG permettra mieux comprendre si le matériel sédimenté dans le centre du Golf et les endroits non frontales sont également productif ou si ils sont fournissent par le zone frontale du sud et ainsi que par la zone frontale du nord.

Un autre aspect à considérer est la taux de sédimentation de particules dans la zone frontal, avec l'objectif de caractériser la qualité du matière organique qu'arrive au fond marin et comment l'export de la matière est influence para les cycles de marées.

Dans cette étude, le transport de nutriments a été évalué en considérant plutôt le transport horizontal de nutriment par l'utilisation des models. Cependant, le transporte vertical avec measures *in vivo* pourrait apporter information pour mieux comprendre la succession de la communauté autotrophe en considérant l'structure vertical de la colonne d'eau et ses instabilités au long d'un cycle de marée vive-eau et morte-eau.

Références bibliographiques

Acha, Eduardo M., Alberto Piola, Oscar Irirbarne, H. M. (2015). Ecological Processes at Marine Fronts Oases in the Ocean. New York: Springer International Publishing AG Switzerland is part of Springer Science+Business Media. Retrieved from www.springer.com. 68pp.

Akselman, R. (1996). Estudios ecológicos en el Golfo San Jorge y adyacencias (Atlántico Sudoccidental): Distribución, abundancia y variación estacional del fitoplancton en relación a factores Físico-químicos y la dinámica hidrológica (Doctoral dissertation, Facultad de Ciencias Exactas y Naturales. Universidad de Buenos Aires).

Aubone A, S Bezzi, R Castrucci, C Dato, P Ibáñez, G Irusta, M Perez, M Renzi, B Santos, N Scarlato, M Simonazzi, L Tringalli & F Villarino. 2000. Merluza (Merluccius hubbsi). In: Bezzi S, R Akselman & E Boschi (eds), Síntesis del estado de las Pesquerías Marítimas Argentinas y de la Cuenca del Plata. Años 1997-1998, con la actualización de 1999: 29-39. INIDEP, Mar del Plata, Argentina.

Bakun, A. (2006). Fronts and eddies as key structures in the habitat of marine fish larvae: opportunity, adaptive response and competitive advantage. Scientia Marina, 70S2 (October), 105–122. http://doi.org/10.3989/scimar.2006.70s2105

Belzile, C., & Gosselin, M. (2015). Free-living stage of the unicellular algae Coccomyxa sp. parasite of the blue mussel (Mytilus edulis): Low-light adaptation, capacity for growth at a very wide salinity range and tolerance to low pH. Journal of invertebrate pathology, 132, 201-207.

Belzile, C., Brugel, S., Nozais, C., Gratton, Y., & Demers, S. (2008). Variations of the abundance and nucleic acid content of heterotrophic bacteria in Beaufort Shelf waters during winter and spring. Journal of Marine Systems, 74(3), 946-956.

Bertilsson, S., Berglund, O., Karl, D. M., & Chisholm, S. W. (2003). Elemental composition of marine Prochlorococcus and Synechococcus: Implications for the ecological stoichiometry of the sea. Limnology and Oceanography, 48(5), 1721–1731.

Bogazzi, E., Baldoni, A., Rivas, A., Martos, P., Reta, R., Orensanz, J. M., … Werner, F. (2005). Spatial correspondence between areas of concentration of Patagonian scallop (Zygochlamys patagonica) and frontal systems in the southwestern Atlantic. Fisheries Oceanography, 14(5), 359–376. http://doi.org/10.1111/j.1365-2419.2005.00340.x

Børsheim, K. Y., & Bratbak, G. (1987). Cell volume to cell carbon conversion factors for a bacterivorous Monas sp. enriched from seawater. Marine Ecology Progress Series, 171-175.

Caron, D. A., Dam, H. G., Kremer, P., Lessard, E. J., Madin, L. P., Malone, T. C., ... & Youngbluth, M. J. (1995). The contribution of microorganisms to particulate carbon and nitrogen in surface waters of the Sargasso Sea near Bermuda. Deep Sea Research Part I: Oceanographic Research Papers, 42(6), 943-972.

Cloern, J. E. (1996). Phytoplankton bloom dynamics in coastal ecosystems: a review with some general lessons from sustained investigation of San Francisco Bay, California. Reviews of Geophysics, 34(2), 127-168.

Copin-Montegut, C., & Copin-Montegut, G. (1983). Stoichiometry of carbon, nitrogen, and phosphorus in marine particulate matter. Deep Sea Research Part A. Oceanographic Research Papers, 30(1), 31-46.

Cucchi-Colleoni & D.Carreto, J. I. (2001).Variación estacional de la biomasa fitoplanctónica en el Golfo San Jorge. Resultados de las Campañas de Investigación OB -01/00,OB-03/00 OB-07/00,OB-10/00 yOB-12/00 Inf.Téc.Int.INIDEP. 30 pp.

Falkowski, P. G. (1980). Light-shade adaptation in marine phytoplankton. In Primary productivity in the sea (pp. 99-119). Springer US.

Fernández, M., Carreto, J. I., Mora, J., & Roux, A. (2005). Physico-chemical characterization of the benthic environment of the Golfo San Jorge, Argentina. Journal of the Marine Biological Association of the United Kingdom, 85(6), 1317-1328.

Fernández, M., Mora, J., Roux, A., Cucchi Colleoni, D. a., & Gasparoni, J. C. (2008). New contribution on spatial and seasonal variability of environmental conditions of the Golfo San Jorge benthic system, Argentina. Journal of the Marine Biological Association of the UK, 88(2), 227–236. http://doi.org/10.1017/S0025315408000465

Franks, P. J. (1992). Phytoplankton blooms at fronts: patterns, scales, and physical forcing mechanisms. Reviews in Aquatic Sciences, 6(2), 121-137.

Geider, R., & La. Roche, J. (2002). Redfield revisited: variability of C:N:P in marine microalgae and its biochemical basis, European Journal of Phycology, 37:1, 1-17,DOI:10.1017/S0967026201003456

Glembocki, N. G., Williams, G. N., Góngora, M. E., Gagliardini, D. A., & Orensanz, J. M. L. (2015). Synoptic oceanography of San Jorge Gulf (Argentina): A template for Patagonian red shrimp (Pleoticus muelleri) spatial dynamics. Journal of Sea Research, 95, 22-35.

Glibert, P. M. (2016). Margalef revisited: A new phytoplankton mandala incorporating twelve dimensions, including nutritional physiology. Harmful Algae, 55, 25-30.

Glorioso, P. D., & Flather, R. A. (1995). A barotropic model of the currents off SE South America, 100(95), 427–440.

Green, J. S. A. (1970). Transfer properties of the large - scale eddies and the general circulation of the atmosphere. Quarterly Journal of the Royal Meteorological Society, 96, 157–185.

Hillebrand, H., Dürselen, C.-D., Kirschtel, D., Pollingher, U., & Zohary, T. (1999). Biovolume Calculation for Pelagic and Benthic Microalgae 1. J. Phycol, 35, 403–424. http://doi.org/10.1046/j.1529-8817.1999.3520403.x

Holligan, P. M., & Mardell, G. T. (1979). Phytoplankton growth and cyclonic eddies. Nature, 278(5701), 245-247.

Kirk, J. T. O. (1994). Light and Photosynthesis in Aquatic systems Cambridge University Press. Cambridge, UK.

Krock, B., Borel, C. M., Barrera, F., Tillmann, U., Fabro, E., Almandoz, G. O., ... & Lara, R. (2015). Analysis of the hydrographic conditions and cyst beds in the San Jorge Gulf, Argentina, that favor dinoflagellate population development including toxigenic species and their toxins. Journal of Marine Systems, 148, 86-100.

Landeira, J. M., Ferron, B., Lunven, M., Morin, P., Marie, L., & Sourisseau, M. (2014). Biophysical interactions control the size and abundance of large phytoplankton chains at the ushant tidal front. PLoS ONE, 9(2). http://doi.org/10.1371/journal.pone.0090507

Li, Q. P., Franks, P. J., Ohman, M. D., & Landry, M. R. (2012). Enhanced nitrate fluxes and biological processes at a frontal zone in the southern California current system. Journal of plankton research, 34(9), 790-801.

Loder, J. W., & Platt, T. (1985). Physical controls on phytoplankton production at tidal fronts. Proceedings Of The Nineteenth European Marine Biology Symposium: Plymouth, Devon, U.K., 16 21 September 1984.Gibbs, P.E.ed, (January 1985), 3–22.

Louge, E. B., Reta, R., Santos, B. a, & Hernandez, D. R. (2004). Variaciones interanuales (1995-2000) de la temperatura y la salinidad registradas en los meses de enero en el Golfo San Jorge y aguas adyacentes (43S-47S). Revista de Investigacion Y Desarrollo Pesquero, 16(Contribucion INIDEP 1275), 27–42.

Mann, K. H., & Lazier, J. R. N. (1996). Dynamics of marine ecosystems: Biological-Physical Interactions in the oceans.

Margalef, R. (1978). Life-forms of phytoplankton as survival alternatives in an unstable environment. Oceanologica, 1(4), 337–341. http://doi.org/10.1590/S0102-09352000000400008

Massé-Beaulne, V., Ferreyra, G. A., Winkler, G., and Nozais, C. (2017). Métabolisme de la communauté microbienne et flux de carbone à court terme dans le golfe San Jorge, Patagonie (Argentine). (Mémoire de maîtrise). Université de Québec à Rimouski/Institut des sciences de la mer de Rimouski.
Maxwell, K., & Johnson, G. N. (2000). Chlorophyll fluorescence-a practical guide. Journal of Experimental Botany, 51(345), 659–668. https://doi.org/10.1093/jexbot/51.345.659

McDougall, T. J., & Barker, P. M. (2011). Getting started with TEOS-10 and the Gibbs Seawater (GSW) oceanographic toolbox. SCOR/IAPSO WG, 127, 1-28.

Menden-Deuer, S., & Lessard, E. J. (2000). Carbon to volume relationships for dinoflagellates, diatoms, and other protist plankton. Limnology and Oceanography, 45(3), 569–579. http://doi.org/10.4319/lo.2000.45.3.0569

Misra, A. N., Misra, M., & Singh, R. (2012). Chlorophyll Fluorescence in Plant Biology. In Biophysics, 220. https://doi.org/10.5772/35111
Moore, C. M., Suggett, D. J., Hickman, A. E., Kim, Y. N., Tweddle, J. F., Sharples, J., ... & Holligan, P. M. (2006). Phytoplankton photoacclimation and photoadaptation in response to environmental gradients in a shelf sea. Limnology and Oceanography, 51(2), 936-949.

Moreira, D., Simionato, C. G., & Dragani, W. (2011). Modeling Ocean Tides and Their Energetics in the North Patagonia Gulfs of Argentina. Journal of Coastal Research, 27(1), 87–102. http://doi.org/10.2112/JCOASTRES-D-09-00055.1

Olenina, I. (2006). Biovolumes and size-classes of phytoplankton in the Baltic Sea. 142p.

Owen, R. (1981). Fronts and Eddies in the Sea: Mechanisms, Interactions, and Biological Effects. Analysis of Marine Ecosystems, 197–233. Retrieved from http://swfsc.noaa.gov/publications/cr/1981/8149.pdf., 1978

Oxborough, K., Moore, C. M., Suggett, D. J., Lawson, T., Chan, H. G., & Geider, R. J. (2012). Direct estimation of functional PSII reaction center concentration and PSII electron flux on a volume basis: a new approach to the analysis of Fast Repetition Rate fluorometry (FRRf) data. Limnology and Oceanography: Methods, 10, 142–154. http://doi.org/10.4319/lom.2012.10.142

Palma, E. D., Matano, R. P., & Piola, A. R. (2004). A numerical study of the Southwestern Atlantic Shelf circulation: Barotropic response to tidal and wind forcing. Journal of Geophysical Research C: Oceans, 109(8), 1–17. http://doi.org/10.1029/2004JC002315

Palma, E. D., Matano, R. P., & Piola, A. R. (2008). A numerical study of the Southwestern Atlantic Shelf circulation: Stratified ocean response to local and offshore forcing. Journal of Geophysical Research: Oceans, 113(C11).

Paparazzo, F. E., Williams, G. N., Pisoni, J. P., Solís, M., Esteves, J. L., & Varela, D. E. (2017). Linking phytoplankton nitrogen uptake, macronutrients and chlorophyll- a in SW Atlantic waters: The case of the Gulf of San Jorge, Argentina. Journal of Marine Systems, 172, 43–50. http://doi.org/10.1016/j.jmarsys.2017.02.007

Parsons, T.R., Maita, Y., Lalli, C.M. (1984). A manual of chemical and biological methods for seawater analysis. Toronto, Pergamon Press. 173p.

Pingree, R. D. (1979). Baroclinic Eddies Bordering The Celtic Sea In Late Summer. Journal of the Marine Biological Association of the United Kingdom, 59(3), 689–698. http://doi.org/10.1017/s0025315400045677

Pingree, R. D., Holligan, P. M., & Mardell, G. T. (1978). The effects of vertical stability on phytoplankton distributions in the summer on the northwest European Shelf. Deep-Sea Research, 25(11). http://doi.org/10.1016/0146-6291(78)90584-2

Pingree, R. D., Holligan, P. M., & Mardell, G. T. (1979). Phytoplankton growth and cyclonic eddies. Nature, 278(5701), 245-247.

R Core Team (2015). R: A language and environment for statistical computing. R Foundation for Statistical Computing, Vienna, Austria. URL https://www.R-project.org/

Redfield, A.C. (1934). On the proportions of organic derivatives in sea water and their relation to the composition of plankton. In James Johnstone Memorial Volume (Daniel, R.J., editor), pp. 176–192. University of Liverpool

Reynolds, C. S. (2006). The ecology of phytoplankton. Cambridge University Press. 435pp.

Rivas, A. L. (1997). Current-meter observations in the Argentine Continental Shelf. Continental Shelf Research, 17(4), 391-406.

Rivas, A. L., & Pisoni, J. P. (2010). Identification, characteristics and seasonal evolution of surface thermal fronts in the Argentinean Continental Shelf. Journal of Marine Systems, 79(1–2), 134–143. http://doi.org/10.1016/j.jmarsys.2009.07.008

Rodriguez, J., Tintoré, J., Allen, J. T., & Blanco, J. M. (2001). Mesoscale vertical motion and the size structure of phytoplankton in the ocean. Nature, 410(6826), 360.

Simpson, J. H., & Hunter, J. R. (1974). Fronts in the Irish Sea. Nature, 250(5465), 404–406. http://doi.org/10.1038/250404a0

Skalar Analytical, B. V. (2005). The SANplus segmented flow analyser: soil and plant analysis. Skalar Analytical BV: Netherlands.

Stewart, Robert H.(2008).Introduction to physical oceanography.Robert H. Stewart.Available electronically from http : //hdl.handle.net/1969.1/160216.

Strickland, J. D. H. and T. R. Parsons. (1972). A practical handbook of seawater analysis. Bull. Fish. Res. Bd. Can., 167, 310 pp.

Suggett DJ, Moore CM, Hickman AE, Geider RJ (2009) Interpretation of fast repetition rate (FRR) fluorescence: signatures of phytoplankton community structure versus physiological state. Mar Ecol Prog Ser 376:1-19. https://doi.org/10.3354/meps07830

Sverdrup, H. U. (1953). On conditions for the vernal blooming of phytoplankton. Journal du Conseil, 18(3), 287-295.

Talley, L. D. (2011). Descriptive physical oceanography: an introduction. Academic press.615pp.

Tarran GA, Heywood JL, Zubkov MV (2006) Latitudinal changes in the standing stocks of nano- and picoeukaryotic phytoplankton in the Atlantic Ocean. Deep-Sea Res II 53: 1516−1529

Tonini M., Palma E., & A. Rivas. (2006). Modelo de alta resolucion de los golfos patagonicos. Asociacion Argentina de Mecanica Computacional, XXV, 1441–1460. http://doi.org/10.1017/CBO9781107415324.004

Townsend, D. W., & Pettigrew, N. R. (1997). Nitrogen limitation of secondary production on Georges Bank. Journal of Plankton Research, 19(2), 221-235

Townsend, D. W., & Thomas, M. (2002). Springtime nutrient and phytoplankton dynamics on Georges Bank. Marine Ecology Progress Series, 228, 57–74. http://doi.org/10.3354/meps228057

Tremblay, G., Belzile, C., Gosselin, M., Poulin, M., Roy, S., & Tremblay, J. É. (2009). Late summer phytoplankton distribution along a 3500 km transect in Canadian Arctic waters: strong numerical dominance by picoeukaryotes. Aquatic Microbial Ecology, 54(1), 55-70.

Utermöhl H. (1958). Zur Vervollkommnung der quantitativen Phytoplankton-Methodik. Mitt Int Ver Theor Angew Limnol 9: 1−38.

Yorio, P. (2009). Marine protected areas, spatial scales, and governance: implications for the conservation of breeding seabirds. Conservation Letters, 2(4), 171–178. http://doi.org/10.1111/j.1755-263X.2009.00062.x

Yorio, P., Quintana, F., Dell 'arciprete, P., & Gonz Lez-Zevallos, D. (2010). Spatial overlap between foraging seabirds and trawl fisheries: implications for the effectiveness of a marine protected area at Golfo San Jorge, Argentina. Bird Conservation International BirdLife International, 20, 320–334. http://doi.org/10.1017/S0959270910000286

Zubkov, M. V., Sleigh, M. A., & Burkill, P. H. (2000). Assaying picoplankton distribution by flow cytometry of underway samples collected along a meridional transect across the Atlantic Ocean. Aquatic Microbial Ecology, 21(1), 13–20. http://doi.org/10.3354/ame021013

9. Annexe

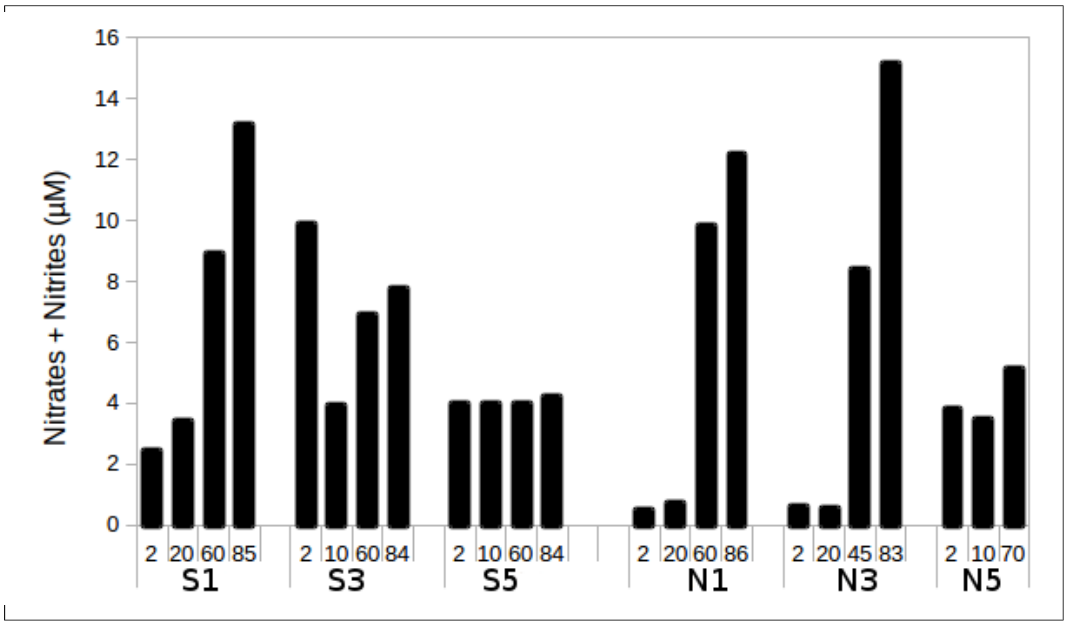

Figure 20: Nitrates + Nitrites concentrations (µM) at different depths (2, 10, 20, 45, 60, 70, 83, 84, 85, 86 m) and at each station, with two measurements above and two below the pycnocline depth.

Figure 11b: linear regression between N:P ratio and the maximum value of Brunt-Väisälä frequency at each station.	Estimate Std. Error t value Pr(>|t|) (Intercept) 5.8268 0.6834 8.526 0.00104 ** X-axe -5117.2631 1291.4126 -3.963 0.01664 * Residual standard error: 0.9844 on 4 degrees of freedom Multiple R-squared: 0.797; Adjusted R-squared: 0.7462 F-statistic: 15.7 on 1 and 4 DF, p-value: 0.01664
Figure 12: C:N ratio as a function of the maximum value of Brunt - Väisälä frequency at each station.	Estimate Std. Error t value Pr(>|t|) (Intercept) 6.570 1.052 6.244 0.00335 ** X-axe -4413.713 1988.354 -2.220 0.09063 . Residual standard error: 1.516 on 4 degrees of freedom Multiple R-squared: 0.5519; Adjusted R-squared: 0.4399 F-statistic: 4.927 on 1 and 4 DF, p-value: 0.09063
Figure 17 (a) lineal regression between POC and autotrophes biomass.	Estimate Std. Error t value Pr(>|t|) (Intercept) 105.5870 19.1827 5.504 0.00531 ** X-axe 1.4846 0.3086 4.811 0.00858 ** Residual standard error: 18.93 on 4 degrees of freedom Multiple R-squared: 0.8526; Adjusted R-squared: 0.8158 F-statistic: 23.14 on 1 and 4 DF, p-value: 0.00858
Figure 17 (b) POC and autotrophes + heterotrophes biomass.	Estimate Std. Error t value Pr(>|t|) (Intercept) 94.0106 17.4700 5.381 0.00576 ** X-axe 1.1923 0.2016 5.915 0.00409 ** Residual standard error: 15.8 on 4 degrees of freedom Multiple R-squared: 0.8974; Adjusted R-squared: 0.8718 F-statistic: 34.99 on 1 and 4 DF, p-value: 0.00409

Table 3: Regression coefficients analyzed with R-studio: residual standard error, R-squared, F- statistic and p-value. (Signif. Codes: 0 ‘***’ 0.001 ‘**’ 0.01 ‘*’ 0.05 ‘.’ 0.1 ‘ ’ 1).